Inverse substructure method for model updating of structures

Shun Weng[1, 2], **Yong Xia***[1], **Xiao-Qing Zhou**[3], **You-Lin Xu**[1], and **Hong-Ping Zhu**[2]

[1] Department of Civil & Structural Engineering, The Hong Kong Polytechnic University, Hong Kong
[2] School of Civil Engineering & Mechanics, Huazhong University of Science and Technology, Wuhan, P. R. China
[3] College of Civil Engineering, Shenzhen University, Shenzhen, P. R. China.
(* Corresponding author, ceyxia@polyu.edu.hk)

Abstract

Traditional model updating of large-scale structures is usually time-consuming because the global structural model needs to be repeatedly re-analyzed as a whole to match global measurements. This paper proposes a new substructural model updating method. The modal data measured on the global structure are disassembled to obtain the independent substructural dynamic flexibility matrices under force and displacement compatibility conditions. The method is extended to the case when the measurement is carried out at partial degrees-of-freedom of the structure. The extracted substructural flexibility matrices are then used as references for updating the corresponding substructural models. An orthogonal projector is employed on both the extracted substructural measurements and the substructural models to remove the rigid body modes of the free-free substructures. Compared with the traditional model updating at the global structure level, only the sub-models at the substructural level are re-analyzed in the proposed substructure-based model updating process, resulting in a rapid convergence of optimization. Moreover, only measurement on the local area corresponding to the concerned substructures is required, and those on other components can be avoided. The effectiveness and efficiency of the proposed substructuring method are verified through applications to a laboratory-tested frame structure and a large-scale 600 m tall Guangzhou New TV Tower. The present technique is referred to as the inverse substructuring model updating method as the measured global modal data are disassembled into the substructure level and then the updating is conducted on the substructures only. This differs from the substructuring model updating method previously

proposed by the authors, in which the model updating is still conducted in the global level and the numerical global modal data are assembled from those of substructures. That can be referred to as the forward substructuring model updating method.

Keywords: Model updating, Substructuring method, Modal flexibility matrix, Damage detection.

1 Introduction

In vibration-based model updating, the finite element (FE) model is iteratively modified to ensure that its vibration properties optimally reproduce the measured counterparts [1]. The FE model of a large-scale structure usually consists of a large number of degrees-of-freedom (DOFs) and many uncertain parameters, which make the conventional model updating method expensive in terms of computation time and computer memory. Xia et al. [2] carried out a model updating exercise for the Balla Balla Bridge in Western Australia; the bridge was modeled with 907 elements, 949 nodes, and 5,400 DOFs. Optimization convergence took 155 iterations and took about 420 hours. In another study, a fine FE model of the Tsing Ma Suspension Bridge consists of about 300,000 nodes, 450,000 elements, and 1.2 million DOFs. About five hours was spent to obtain the first 100 eigensolutions using a 64-bit Itanium server with eight CPUs of 1.5 GHz each [3]. In such a case, updating the FE model using the conventional approach is very difficult, even with a powerful computer.

The substructuring approach is potentially efficient in the model updating of large-scale structures [4-7] and related applications [8-10]. In these studies, the global structure is divided into smaller and more manageable substructures. The substructures are analyzed independently to obtain their designated solutions, which are then assembled to recover the solutions to the global structure by imposing constraints at the interfaces. The substructure-based model updating presents the following advantages: 1) it enables considerably easier and faster analysis of small

system matrices; 2) only the substructures need to be updated and re-analyzed instead of analyzing the global structure; 3) the substructuring method can be more efficient when it is incorporated with parallel computation.

Nevertheless, the substructure-based model updating method requires the repeated assembly of the vibration properties (e.g., frequencies and mode shapes) of the substructural FE models into global vibration properties; the assembled properties are then compared with the global measurements. In the present paper, we develop a new substructure-based model updating method, in which the iterative updating process is performed within the substructures only. To achieve this, the global measurements are disassembled into the vibration properties of the substructures. Subsequently, the substructural measurements are used as references for updating the corresponding substructural FE models via the conventional model updating procedure. The proposed inverse process is referred to as the inverse substructuring method, whereas the previous approach can be referred to as the forward substructuring method.

The inverse substructuring method involves the identification of substructural properties. Alvin and Park [11] proposed a force method for the extraction of substructural flexibility matrices from the global flexibility matrix. Doebling and Peterson [12] disassembled the measured global stiffness matrix or flexibility matrix into a substructural stiffness. Apart from the frequency domain, Koh et al. [13] and Law et al. [14] identified substructural properties in the time domain. In these substructuring approaches, the modal data of the global structure required measurement on all the DOFs of the structures, thereby limiting the application to large-scale structures. Moreover, the studies focus on small structures and numerical examples only. Developing an effective scheme that can be applied to large-scale structures is necessary.

In the current work, the inverse substructuring approach is developed for structural model updating. The substructural dynamic flexibility matrices are extracted from the experimental modal properties of the global structure. An orthogonal projector is employed to remove the rigid

body modes of the independent free-free substructures. Furthermore, the proposed substructuring method is extended to a practical case in which only partial DOFs are measured. The substructural models are then independently updated so that the dynamic flexibility matrices match the extracted ones from the measurement.

The proposed method is applied to a small laboratory-tested structure and a large-scale supertall structure. The results demonstrate that the proposed inverse substructuring model updating method is more accurate and effective compared with the conventional approach.

2 Disassembly of global flexibility with full DOF measurement

In this section, the flexibility of the global structure is disassembled to the substructural level. The flexibility matrix of the global structure is formulated from its vibration properties as

$$\mathbf{F}_g = \mathbf{\Phi}_d \left(\mathbf{\Lambda}_d \right)^{-1} \left[\mathbf{\Phi}_d \right]^T \tag{1}$$

where $\mathbf{\Lambda}_d$ is a diagonal matrix whose elements are the measured eigenvalues, $\mathbf{\Phi}_d$ is the corresponding mass-normalized deformational mode shapes, and $\mathbf{F}_g$ is the flexibility matrix of the global structure. Subscript g represents the variables in the original global structure before disassembly. The global flexibility matrix can be formulated with sufficient accuracy using a few of the lowest measured modes [15-16].

The substructuring method divides the global structure into independent free or fixed substructures. Without loss of generality, a global structure with N DOFs is divided into two substrctures: a fixed-free substructure of $N^{(1)}$ DOFs (Substructure 1) and a free-free substructure of $N^{(2)}$ DOFs (Substructure 2), connected by N_B interface DOFs (Fig. 1). The partitioned substructures have DOFs of $NP = N^{(1)} + N^{(2)} = N + N_B$ in total.

The flexibility matrix of a fixed-free substructure, such as Substructure 1 in Fig. 1, is contributed by the deformational modes as

$$\mathbf{F}^{(1)} = \sum_{i=1}^{N_d^{(1)}} \frac{1}{\lambda_i^{(1)}} \left\{\phi_i^{(1)}\right\} \left\{\phi_i^{(1)}\right\}^T = \mathbf{\Phi}_d^{(1)} \left[\mathbf{\Lambda}_d^{(1)}\right]^{-1} \left[\mathbf{\Phi}_d^{(1)}\right]^T \tag{2}$$

where $\lambda_i^{(1)}$ is the *i*th eigenvalues of Substructure 1, and $\left\{\phi_i^{(1)}\right\}$ denotes the *i*th eigenvector. The flexibility matrix contributed by the deformational modes is also called modal flexibility.

The flexibility matrix of a free substructure does not exist because of the rigid body motion, which corresponds to zero eigenvalues. Considering the contribution from both rigid body modes and deformational modes, a generalized flexibility matrix is then defined here as [17-18]

$$\overline{\mathbf{F}}^{(2)} = \sum_{i=1}^{N_d^{(2)}} \frac{1}{\lambda_i^{(2)}} \left\{\phi_i^{(2)}\right\} \left\{\phi_i^{(2)}\right\}^T + \sum_{r=1}^{N_r^{(2)}} \alpha_r^{(2)} \left\{\phi_r^{(2)}\right\} \left\{\phi_r^{(2)}\right\}^T = \mathbf{\Phi}_d^{(2)} \left[\mathbf{\Lambda}_d^{(2)}\right]^{-1} \left[\mathbf{\Phi}_d^{(2)}\right]^T + \mathbf{R}^{(2)} \mathbf{A}^{(2)} \left[\mathbf{R}^{(2)}\right]^T \tag{3}$$

where $\lambda_i^{(2)}$ and $\left\{\phi_i^{(2)}\right\}$ are the deformational eigenpairs of Substructure 2; $\mathbf{R}^{(2)} = \left[\left\{\phi_1^{(2)}\right\}, \left\{\phi_2^{(2)}\right\}, ..., \left\{\phi_{N_r}^{(2)}\right\}\right]$ denotes the rigid body modes; $\mathbf{A}^{(2)} = Diag\left(\left\{\alpha_1^{(2)}, \alpha_2^{(2)}, ..., \alpha_{N_r}^{(2)}\right\}\right)$ represents the participation factors of the rigid body modes; Subscripts *d* and *r* denote the variables associated with the deformational and rigid body modes, respectively. For a free substructure, the modal flexibility matrix is contributed solely by the deformational modes as

$$\mathbf{F}^{(2)} = \sum_{i=1}^{N_d^{(2)}} \frac{1}{\lambda_i^{(2)}} \left\{\phi_i^{(2)}\right\} \left\{\phi_i^{(2)}\right\}^T = \mathbf{\Phi}_d^{(2)} \left[\mathbf{\Lambda}_d^{(2)}\right]^{-1} \left[\mathbf{\Phi}_d^{(2)}\right]^T \tag{4}$$

To be independent substructures, the substructural variables are written in primitive forms

$$\left\{x^p\right\} = \begin{Bmatrix} x^{(1)} \\ x^{(2)} \end{Bmatrix}, \quad \left\{f^p\right\} = \begin{Bmatrix} f^{(1)} \\ f^{(2)} \end{Bmatrix}$$

$$\mathbf{K}^p = \begin{bmatrix} \mathbf{K}^{(1)} & \mathbf{0} \\ \mathbf{0} & \mathbf{K}^{(2)} \end{bmatrix}, \quad \mathbf{F}^p = \begin{bmatrix} \mathbf{F}^{(1)} & \mathbf{0} \\ \mathbf{0} & \overline{\mathbf{F}}^{(2)} \end{bmatrix}, \quad \mathbf{R}^p = \begin{bmatrix} \mathbf{R}^{(1)} & \mathbf{0} \\ \mathbf{0} & \mathbf{R}^{(2)} \end{bmatrix} = \begin{bmatrix} \mathbf{0} \\ \mathbf{R}^{(2)} \end{bmatrix} \tag{5}$$

where **K**, **F**, *x*, and *f* represent the stiffness matrix, flexibility matrix, nodal displacements, and external forces, respectively. Here the rigid body mode of the first substructure is null. Superscript *p* denotes the primitive matrices or vectors, which directly encompass the variables of the independent substructures without imposing any constraints on them. The primitive

matrices or vectors take length *NP*.

Let $\{x_g\}$ denote the nodal displacement vector of the global structure and $\{f_g\}$ the external force vector. The primitive forms of the substructural displacements and forces are linked to the global displacement and force vectors by

$$\left\{x^p\right\} = \mathbf{L}^p \left\{x_g\right\} \tag{6}$$

$$\left[\mathbf{L}^p\right]^T \left\{f^p\right\} = \left\{f_g\right\} \tag{7}$$

where $\mathbf{L}^p$ is the geometric operator with size $NP \times N$, and is determined by the geometric relationship between the substructures and the global structure. For example, if the *j*th DOF of the global structure corresponds to the *i*th DOF in the separated substructures, then $\mathbf{L}_{ij}^p = 1$.

The displacement of an independent substructure can be written as a superposition of its deformational and rigid body motions [11] as follows.

$$\left\{x^p\right\} = \mathbf{F}^p \left\{f^p\right\} + \mathbf{R}^p \left\{\alpha^p\right\} \tag{8}$$

where $\left\{f^p\right\}$ represents the forces imposed on the independent substructures. The primitive forms of the rigid body modes and forces satisfy the force equilibrium compatibility equation

$$\left[\mathbf{R}^p\right]^T \left\{f^p\right\} = \{\mathbf{0}\} \tag{9}$$

As an independent structure, a substructure is loaded by the external force and the connecting force from the adjacent substructures as

$$\left\{f^p\right\} = \left(\left[\mathbf{L}^p\right]^T\right)^+ \left\{f_g\right\} + \mathbf{C}\{\tau\} = \left\{\tilde{f}_g\right\} + \mathbf{C}\{\tau\} \tag{10}$$

where $\left\{\tilde{f}_g\right\} = \left(\left[\mathbf{L}^p\right]^T\right)^+ \left\{f_g\right\} = \tilde{\mathbf{L}}^p \left\{f_g\right\}$, $\tilde{\mathbf{L}}^p = \left(\left[\mathbf{L}^p\right]^T\right)^+$ is the generalized inverse of $\left[\mathbf{L}^p\right]^T$; $\{\tau\}$ is the Lagrange multiplier representing the connecting forces along the interfaces of the substructures; and matrix **C** implicitly defines the general connections between the independent substructures. In matrix **C**, each row contains two non-zero elements, 1 and –1, for a rigid connection. From the physical perspective, matrix **C** bears the displacement compatibility [4, 19]

$$\mathbf{C}^T \left\{ x^p \right\} = \{\mathbf{0}\} \tag{11}$$

The substitution of Eq. (10) into Eq. (8) yields

$$\left\{ x^p \right\} = \mathbf{F}^p \left(\left\{ \tilde{f}_g \right\} + \mathbf{C}\{\tau\} \right) + \mathbf{R}^p \left\{ \alpha^p \right\} \tag{12}$$

From Eq. (6), the global displacement can be expressed by the substructural variables as

$$\left\{ x_g \right\} = \left[\mathbf{L}^p \right]^+ \left\{ x^p \right\} = \left[\tilde{\mathbf{L}}^p \right]^T \mathbf{F}^p \left(\left\{ \tilde{f}_g \right\} + \mathbf{C}\{\tau\} \right) + \left[\tilde{\mathbf{L}}^p \right]^T \mathbf{R}^p \left\{ \alpha^p \right\} \tag{13}$$

Given that the global displacement and force vectors satisfy $\left\{ x_g \right\} = \mathbf{F}_g \left\{ f_g \right\}$, Eq. (13) is employed to relate substructural flexibility matrix $\mathbf{F}^p$ to global flexibility matrix $\mathbf{F}_g$. To achieve this, force compatibility Eq. (9) and displacement compatibility Eq. (11) are employed to solve the variables $\{\tau\}$ and $\left\{ \alpha^p \right\}$ in Eq. (13). The substitution of Eq. (10) into Eq. (9) yields

$$\left[\mathbf{R}^p \right]^T \left(\left\{ \tilde{f}_g \right\} + \mathbf{C}\{\tau\} \right) = \{\mathbf{0}\} \tag{14}$$

Substituting Eq. (12) into Eq. (11) leads to

$$\mathbf{C}^T \left[\mathbf{F}^p \left(\left\{ \tilde{f}_g \right\} + \mathbf{C}\{\tau\} \right) + \mathbf{R}^p \left\{ \alpha^p \right\} \right] = \{\mathbf{0}\} \tag{15}$$

From Eq. (15), $\{\tau\}$ is expressed as

$$\{\tau\} = -\mathbf{F}_C^{-1} \left(\mathbf{C}^T \mathbf{F}^p \left\{ \tilde{f}_g \right\} + \mathbf{R}_C \left\{ \alpha^p \right\} \right) \tag{16}$$

where

$$\mathbf{F}_C = \mathbf{C}^T \mathbf{F}^p \mathbf{C}, \quad \mathbf{R}_C = \mathbf{C}^T \mathbf{R}^p \tag{17}$$

The substitution of Eq. (16) into Eq. (14) yields

$$\left\{ \alpha^p \right\} = \mathbf{K}_R^{-1} \left(\left[\mathbf{R}^p \right]^T - \mathbf{R}_C^T \mathbf{F}_C^{-1} \mathbf{C}^T \mathbf{F}^p \right) \left\{ \tilde{f}_g \right\} \tag{18}$$

where $\mathbf{K}_R = \mathbf{R}_C^T \mathbf{F}_C^{-1} \mathbf{R}_C$. Substituting Eq. (18) into Eq. (16), $\{\tau\}$ is solved thus:

$$\{\tau\} = -\mathbf{F}_C^{-1} \mathbf{C}^T \mathbf{F}^p \left\{ \tilde{f}_g \right\} + \mathbf{F}_C^{-1} \mathbf{R}_C \mathbf{K}_R^{-1} \left(\mathbf{R}_C^T \mathbf{F}_C^{-1} \mathbf{C}^T \mathbf{F}^p - \left[\mathbf{R}^p \right]^T \right) \left\{ \tilde{f}_g \right\} \tag{19}$$

As long as $\{\tau\}$ and $\left\{ \alpha^p \right\}$ are solved, Eq. (13) can be expressed as

$$\left\{x_g\right\}=\left[\tilde{\mathbf{L}}^p\right]^T\left(\mathbf{F}^p-\mathbf{F}^p\mathbf{K}_C\mathbf{F}^p+\mathbf{F}^p\mathbf{K}_C\mathbf{F}_R\mathbf{K}_C\mathbf{F}^p-\mathbf{F}^p\mathbf{K}_C\mathbf{F}_R-\mathbf{F}_R\mathbf{K}_C\mathbf{F}^p-\mathbf{F}^p\mathbf{H}\mathbf{F}^p+\mathbf{F}_R\right)\left\{\tilde{f}_g\right\}$$

$$=\left[\tilde{\mathbf{L}}^p\right]^T\left(\mathbf{F}^p-\mathbf{F}^p\mathbf{H}\mathbf{F}^p-\mathbf{F}^p\mathbf{K}_C\mathbf{F}_R-\mathbf{F}_R^T\mathbf{K}_C^T\mathbf{F}^p+\mathbf{F}_R\right)\tilde{\mathbf{L}}^p\left\{f_g\right\} \tag{20}$$

in which

$$\mathbf{F}_R=\mathbf{R}^p\left(\left[\mathbf{R}^p\right]^T\mathbf{K}_C\mathbf{R}^p\right)^{-1}\left[\mathbf{R}^p\right]^T,\ \ \mathbf{H}=\mathbf{K}_C-\mathbf{K}_C\mathbf{F}_R\mathbf{K}_C,\ \ \mathbf{K}_C=\mathbf{C}\mathbf{F}_C^{-1}\mathbf{C}^T$$

Therefore,

$$\mathbf{F}_g=\left[\tilde{\mathbf{L}}^p\right]^T\left(\mathbf{F}^p-\mathbf{F}^p\mathbf{H}\mathbf{F}^p-\mathbf{F}^p\mathbf{K}_C\mathbf{F}_R-\mathbf{F}_R^T\mathbf{K}_C^T\mathbf{F}^p+\mathbf{F}_R\right)\tilde{\mathbf{L}}^p \tag{21}$$

or the global flexibility matrix can be expressed by the substructural flexibility matrix as

$$\mathbf{L}^p\mathbf{F}_g\left[\mathbf{L}^p\right]^T=\mathbf{F}^p-\mathbf{F}^p\mathbf{K}_C\mathbf{F}_R-\mathbf{F}_R^T\mathbf{K}_C^T\mathbf{F}^p-\mathbf{F}^p\mathbf{H}\mathbf{F}^p+\mathbf{F}_R \tag{22}$$

In Eq. (22), substructural flexibility matrix $\mathbf{F}^p$ contributes to global flexibility matrix $\mathbf{F}_g$ in a complicated manner. Expressing $\mathbf{F}^p$ in terms of $\mathbf{F}_g$ in an explicit form is difficult. An iterative scheme is required to obtain substructural flexibility matrix $\mathbf{F}^p$.

Considering the structure in Fig. 1, global flexibility $\mathbf{F}_g$ is disassembled into the substructural flexibility matrices of the two substructures according to the following procedures.

1) The flexibility matrix measured on global structure $\mathbf{F}_g$ is expanded by geometric operator $\mathbf{L}^p$ as

$$\widehat{\mathbf{F}}_g=\mathbf{L}^p\mathbf{F}_g\left[\mathbf{L}^p\right]^T \tag{23}$$

where $\widehat{\mathbf{F}}_g$ takes size $NP\times NP$.

2) The initial value of $\mathbf{F}^p$ is formed from the global flexibility as

$$\left[\mathbf{F}^p\right]^{[0]}=\begin{bmatrix}\widehat{\mathbf{F}}_g\left(0:N^{(1)}\ ,\ 0:N^{(1)}\right) & \mathbf{0}\\ \mathbf{0} & \widehat{\mathbf{F}}_g\left(\left(N^{(1)}+1\right):NP\ ,\ \left(N^{(1)}+1\right):NP\right)\end{bmatrix} \tag{24}$$

3) The substructural flexibility matrix is extracted iteratively using Eq. (22). In the kth iteration,

$$\left[\mathbf{F}_0^p\right]^{[k]}=\widehat{\mathbf{F}}_g+\left[\mathbf{F}^p\right]^{[k-1]}\mathbf{K}_C^{[k-1]}\mathbf{F}_R^{[k-1]}+\left[\mathbf{F}_R^{[k-1]}\right]^T\left[\mathbf{K}_C^{[k-1]}\right]^T\left[\mathbf{F}^p\right]^{[k-1]}+\left[\mathbf{F}^p\right]^{[k-1]}\mathbf{H}^{[k-1]}\left[\mathbf{F}^p\right]^{[k-1]}-\mathbf{F}_R^{[k-1]} \tag{25}$$

To keep the block-diagonal property of $\mathbf{F}^p$, the diagonal sub-blocks of $\left[\mathbf{F}_0^p\right]^{[k]}$ corresponding

to the two substructures are used in the next iteration as follows:

$$\left[\mathbf{F}^{p}\right]^{[k]}=\begin{bmatrix}\left[\mathbf{F}_{0}^{p}\right]^{[k]}\left(0:N^{(1)} \quad , \quad 0:N^{(1)}\right) & \mathbf{0} \\ \mathbf{0} & \left[\mathbf{F}_{0}^{p}\right]^{[k]}\left(\left(N^{(1)}+1\right):NP \quad , \quad \left(N^{(1)}+1\right):NP\right)\end{bmatrix} \tag{26}$$

4) Step 3 is repeated until the relative difference of the substructural flexibility matrices from two consecutive iterations is less than a predefined tolerance, i.e.,

$$e=\frac{norm\left(\left[\mathbf{F}^{p}\right]^{[k]}-\left[\mathbf{F}^{p}\right]^{[k-1]}\right)}{norm\left(\left[\mathbf{F}^{p}\right]^{[k]}\right)}\le Tol \tag{27}$$

The substructural flexibility matrices are therefore the diagonal sub-blocks of $\left[\mathbf{F}^{p}\right]^{[k]}$. The convergence of the iteration will be verified by numerical example in this paper, and the convergence proof in an elegant mathematical sense deserves further study.

For a free substructure, the substructural flexibility matrix extracted from the global flexibility matrix is contributed by both the rigid body modes and deformational modes of the substructure. An orthogonal projector is needed to remove the rigid body component and extract the modal flexibility of a free substructure [17-20]. The construction of the orthogonal projector can be found in the Appendix. The modal flexibility matrix can be used for model updating [16].

3 Disassembly of global flexibility with partial DOF measurement

In practice, a structure is usually measured at the partial DOFs of measurement points. For example, some responses such as rotation are difficult and expensive to measure. If partitioning the full DOFs of the measured points into the measured DOFs (denoted by subscript *a*) and the unmeasured DOFs (denoted by subscript *b*), the full modal flexibility of a structure takes on the expression

$$\mathbf{F}_{g}=\boldsymbol{\Phi}_{d}\boldsymbol{\Lambda}_{d}^{-1}\boldsymbol{\Phi}_{d}^{T}=\begin{bmatrix}\boldsymbol{\Phi}_{ad}\boldsymbol{\Lambda}_{d}^{-1}\boldsymbol{\Phi}_{ad}^{T} & \boldsymbol{\Phi}_{ad}\boldsymbol{\Lambda}_{d}^{-1}\boldsymbol{\Phi}_{bd}^{T} \\ \boldsymbol{\Phi}_{bd}\boldsymbol{\Lambda}_{d}^{-1}\boldsymbol{\Phi}_{ad}^{T} & \boldsymbol{\Phi}_{bd}\boldsymbol{\Lambda}_{d}^{-1}\boldsymbol{\Phi}_{bd}^{T}\end{bmatrix}=\begin{bmatrix}\left(\mathbf{F}_{g}\right)_{aa} & \left(\mathbf{F}_{g}\right)_{ab} \\ \left(\mathbf{F}_{g}\right)_{ba} & \left(\mathbf{F}_{g}\right)_{bb}\end{bmatrix} \tag{28}$$

The partial flexibility matrix estimated at the measured DOFs is directly related to the

corresponding rows and columns of the full flexibility [15].

$$\left(\mathbf{F}_g\right)_{aa} = \boldsymbol{\Phi}_{ad}\left(\boldsymbol{\Lambda}_{ad}\right)^{-1}\left[\boldsymbol{\Phi}_{ad}\right]^T \tag{29}$$

where $\boldsymbol{\Lambda}_{ad}$ and $\boldsymbol{\Phi}_{ad}$ include the natural frequencies and deformational mode shapes estimated at the measured DOFs. In this section, the substructural flexibility is extracted when the global structure is measured at the partial DOFs.

For this purpose, force compatibility Eq. (14) and displacement compatibility Eq. (15) are partitioned into the measured DOFs and unmeasured DOFs as

$$\begin{bmatrix}\mathbf{R}_a^p\\ \mathbf{R}_b^p\end{bmatrix}^T\left(\begin{Bmatrix}\{\tilde{f}_g\}_a\\ \{\tilde{f}_g\}_b\end{Bmatrix}+\begin{bmatrix}\mathbf{C}_a\\ \mathbf{C}_b\end{bmatrix}\{\tau\}\right)=\mathbf{0} \tag{30}$$

$$\begin{bmatrix}\mathbf{C}_a\\ \mathbf{C}_b\end{bmatrix}^T\left(\begin{bmatrix}\mathbf{F}_{aa}^p & \mathbf{F}_{ab}^p\\ \mathbf{F}_{ba}^p & \mathbf{F}_{bb}^p\end{bmatrix}\left(\begin{Bmatrix}\{\tilde{f}_g\}_a\\ \{\tilde{f}_g\}_b\end{Bmatrix}+\begin{bmatrix}\mathbf{C}_a\\ \mathbf{C}_b\end{bmatrix}\{\tau\}\right)+\begin{bmatrix}\mathbf{R}_a^p\\ \mathbf{R}_b^p\end{bmatrix}\{\alpha^p\}\right)=\mathbf{0} \tag{31}$$

Consequently, $\{\tau\}$ is solved from Eq. (31) as

$$\{\tau\}=-\left(\begin{bmatrix}\mathbf{C}_a\\ \mathbf{C}_b\end{bmatrix}^T\begin{bmatrix}\mathbf{F}_{aa}^p & \mathbf{F}_{ab}^p\\ \mathbf{F}_{ba}^p & \mathbf{F}_{bb}^p\end{bmatrix}\begin{bmatrix}\mathbf{C}_a\\ \mathbf{C}_b\end{bmatrix}\right)^{-1}\left(\begin{bmatrix}\mathbf{C}_a\\ \mathbf{C}_b\end{bmatrix}^T\begin{bmatrix}\mathbf{F}_{aa}^p & \mathbf{F}_{ab}^p\\ \mathbf{F}_{ba}^p & \mathbf{F}_{bb}^p\end{bmatrix}\begin{Bmatrix}\{\tilde{f}_g\}_a\\ \{\tilde{f}_g\}_b\end{Bmatrix}+\begin{bmatrix}\mathbf{C}_a\\ \mathbf{C}_b\end{bmatrix}^T\begin{bmatrix}\mathbf{R}_a^p\\ \mathbf{R}_b^p\end{bmatrix}\{\alpha^p\}\right) \tag{32}$$

If the interface DOFs are the measured DOFs, i.e., $\{\tilde{f}_g\}_b=\mathbf{0}$, $\mathbf{C}_b=\mathbf{0}$, and $\{\tilde{f}_g\}_a=\left(\left[\mathbf{L}_{aa}^p\right]^T\right)^+\{f_g\}_a=\tilde{\mathbf{L}}_{aa}^p\{f_g\}_a$, Eq. (32) is simplified to

$$\{\tau\}=-\mathbf{F}_{Ca}^{-1}\left(\mathbf{C}_a^T\mathbf{F}_{aa}^p\{\tilde{f}_g\}_a+\mathbf{C}_a^T\mathbf{R}_a^p\{\alpha^p\}\right) \tag{33}$$

where $\mathbf{F}_{Ca}=\mathbf{C}_a^T\mathbf{F}_{aa}\mathbf{C}_a$. Substituting Eq. (33) into Eq. (30) enables $\{\alpha^p\}$ to be solved as

$$\{\alpha^p\}=\mathbf{K}_{Ra}^{-1}\left(\left[\mathbf{R}_a^p\right]^T-\left[\mathbf{R}_a^p\right]^T\mathbf{C}_a\mathbf{F}_{Ca}^{-1}\mathbf{C}_a^T\mathbf{F}_{aa}^p\right)\{\tilde{f}_g\}_a \tag{34}$$

and $\{\tau\}$ is therefore solved from Eq. (33) thus:

$$\{\tau\}=-\mathbf{F}_{Ca}^{-1}\mathbf{C}_a^T\mathbf{F}_{aa}^p\{\tilde{f}_g\}_a+\mathbf{F}_{Ca}^{-1}\mathbf{C}_a^T\mathbf{R}_a^p\mathbf{K}_{Ra}^{-1}\left(\left[\mathbf{R}_a^p\right]^T\mathbf{K}_{Ca}\mathbf{F}_{aa}^p-\left[\mathbf{R}_a^p\right]^T\right)\{\tilde{f}_g\}_a \tag{35}$$

where $\mathbf{K}_{Ca}=\mathbf{C}_a\mathbf{F}_{Ca}^{-1}\mathbf{C}_a^T$ and $\mathbf{K}_{Ra}=\left[\mathbf{R}_a^p\right]^T\mathbf{K}_{Ca}\mathbf{R}_a^p=\left[\mathbf{R}_a^p\right]^T\mathbf{C}_a\mathbf{F}_{Ca}^{-1}\mathbf{C}_a^T\mathbf{R}_a^p$.

The displacement vector in Eq. (13) is partitioned according to the measured and unmeasured DOFs as

$$\begin{Bmatrix} \{x_g\}_a \\ \{x_g\}_b \end{Bmatrix} = \begin{bmatrix} \tilde{\mathbf{L}}_{aa}^p & \mathbf{0} \\ \mathbf{0} & \tilde{\mathbf{L}}_{bb}^p \end{bmatrix}^T \begin{bmatrix} \mathbf{F}_{aa}^p & \mathbf{F}_{ab}^p \\ \mathbf{F}_{ba}^p & \mathbf{F}_{bb}^p \end{bmatrix} \left(\begin{Bmatrix} \{\tilde{f}_g\}_a \\ \{\tilde{f}_g\}_b \end{Bmatrix} + \begin{bmatrix} \mathbf{C}_a \\ \mathbf{C}_b \end{bmatrix} \{\tau\} \right) + \begin{bmatrix} \tilde{\mathbf{L}}_{aa}^p & \mathbf{0} \\ \mathbf{0} & \tilde{\mathbf{L}}_{bb}^p \end{bmatrix}^T \begin{bmatrix} \mathbf{R}_a^p \\ \mathbf{R}_b^p \end{bmatrix} \{\alpha^p\} \quad (36)$$

The displacements at the measured DOFs are expressed by

$$\{x_g\}_a = \left[\tilde{\mathbf{L}}_{aa}^p\right]^T \mathbf{F}_{aa}^p \left(\{\tilde{f}_g\}_a + \mathbf{C}_a \{\tau\} \right) + \mathbf{R}_a^p \{\alpha^p\} \quad (37)$$

Given the solutions of $\{\alpha^p\}$ in Eq. (34) and $\{\tau\}$ in Eq. (35), the displacement vector of the global structure [Eq. (37)] is thereby expressed as

$$\begin{aligned} \{x_g\}_a = \left[\tilde{\mathbf{L}}_{aa}^p\right]^T \Big(& \mathbf{F}_{aa}^p - \mathbf{F}_{aa}^p \mathbf{K}_{Ca} \mathbf{F}_{aa}^p + \mathbf{F}_{aa}^p \mathbf{K}_{Ca} \mathbf{F}_{Ra} \mathbf{K}_{Ca} \mathbf{F}_{aa}^p \\ & - \mathbf{F}_{aa}^p \mathbf{K}_{Ca} \mathbf{R}_a \mathbf{K}_{Ra}^{-1} \left[\mathbf{R}_a^p\right]^T - \mathbf{R}_a^p \mathbf{K}_{Ra}^{-1} \left[\mathbf{R}_a^p\right]^T \mathbf{K}_{Ca} \mathbf{F}_{aa}^p + \mathbf{R}_a^p \mathbf{K}_{Ra}^{-1} \left[\mathbf{R}_a^p\right]^T \Big) \tilde{\mathbf{L}}_{aa}^p \{f_g\}_a \end{aligned} \quad (38)$$

For the global structure, the displacements are related to the external forces by the global flexibility as

$$\{x_g\} = \begin{Bmatrix} \{x_g\}_a \\ \{x_g\}_b \end{Bmatrix} = \begin{bmatrix} (\mathbf{F}_g)_{aa} & (\mathbf{F}_g)_{ab} \\ (\mathbf{F}_g)_{ba} & (\mathbf{F}_g)_{bb} \end{bmatrix} \begin{Bmatrix} \{f_g\}_a \\ \{f_g\}_b \end{Bmatrix} \quad (39)$$

The partial flexibility matrix corresponding to the measured DOFs is defined as the displacement responses subjected to a unit force applied at the measured DOFs, whereas the forces at the other DOFs are zero, i.e., $\{f_g\}_b = \mathbf{0}$. Consequently, the displacements at the measured DOFs are related to the external forces as

$$\{x_g\}_a = (\mathbf{F}_g)_{aa} \{f_g\}_a \quad (40)$$

Concerning Eqs. (38) and (40), the substructural flexibility and global flexibility at the measured DOFs are linked by

$$\mathbf{L}_{aa}^p (\mathbf{F}_g)_{aa} \left[\mathbf{L}_{aa}^p\right]^T = \mathbf{F}_{aa}^p - \mathbf{F}_{aa}^p \mathbf{K}_{Ca} \mathbf{F}_{aa}^p + \mathbf{F}_{aa}^p \mathbf{K}_{Ca} \mathbf{F}_{Ra} \mathbf{K}_{Ca} \mathbf{F}_{aa}^p$$

$$-\mathbf{F}_{aa}^{p}\mathbf{K}_{Ca}\mathbf{R}_{a}\mathbf{K}_{Ra}^{-1}\left[\mathbf{R}_{a}^{p}\right]^{T}-\mathbf{R}_{a}^{p}\mathbf{K}_{Ra}^{-1}\left[\mathbf{R}_{a}^{p}\right]^{T}\mathbf{K}_{Ca}\mathbf{F}_{aa}^{p}+\mathbf{R}_{a}^{p}\mathbf{K}_{Ra}^{-1}\left[\mathbf{R}_{a}^{p}\right]^{T} \tag{41}$$

i.e.,

$$\mathbf{L}_{aa}^{p}\left(\mathbf{F}_{g}\right)_{aa}\left[\mathbf{L}_{aa}^{p}\right]^{T}=\mathbf{F}_{aa}^{p}-\mathbf{F}_{aa}^{p}\mathbf{H}_{aa}\mathbf{F}_{aa}^{p}-\mathbf{F}_{aa}^{p}\mathbf{K}_{Ca}\mathbf{F}_{Ra}-\mathbf{F}_{Ra}\mathbf{K}_{Ca}\mathbf{F}_{aa}^{p}+\mathbf{F}_{Ra} \tag{42}$$

where $\mathbf{H}_{aa}=\mathbf{K}_{Ca}-\mathbf{K}_{Ca}\mathbf{F}_{Ra}\mathbf{K}_{Ca}$ and $\mathbf{F}_{Ra}=\mathbf{R}_{a}\mathbf{K}_{Ra}^{-1}\left[\mathbf{R}_{a}^{p}\right]^{T}$. With regard to Eq. (42), an iterative scheme is required to calculate partial substructural flexibility $\mathbf{F}_{aa}^{p}$ at the measured DOFs. The iteration procedures are similar to those described in Section 2. In practice, a structure is usually measured at limited DOFs. The matrix involved in the iteration, corresponding to the measured DOFs, has a small size. Consequently the computational expense of the iteration is much smaller than those cost in updating the global model. The latter is usually performed on the FE model with millions of DOFs for a large-scale structure. This will be demonstrated using a large-scale structure in Section 6.

The interface DOFs serve to constrain the independent substructures via the compatibility equations, and should therefore always be selected as the measured DOFs. This is the limitation of the present substructuring method. The unmeasured DOFs of the interface points can be estimated using either the analytical model or the curve fitting approach [21, 22]. Future work is needed to address this shortcoming.

As before, the partial substructural flexibility matrices extracted from the global flexibility matrix include the contribution from both the rigid body modes and deformational modes. The rigid body modes should be removed from the partial substructural flexibility to enable extraction of the modal flexibility for model updating. For this purpose, a condensed orthogonal projector $\mathbf{P}_a$ orthogonal to $\mathbf{R}_a$ is formulated in the Appendix [17, 23]. To make the partial substructural flexibility matrix extracted from the global flexibility and that calculated from the analytical substructural model comparable in the model updating, both are normalized with condensed projector $\mathbf{P}_a$.

In the proposed substructuring method, the substructural flexibility matrices in primitive matrix $\mathbf{F}_{aa}^{p}$ are independent. The substructural flexibility matrices can be simultaneously extracted from the global flexibility for all substructures, or be extracted for one or more specific substructures. In the former, the global structure is measured and the substructural flexibility matrices of all the substructures can be simultaneously obtained at the points corresponding to the measured DOFs. In the latter, only the local area of the concerned substructure needs to be measured in the experiment, and the substructural flexibility matrix of the concerned substructure is accordingly extracted.

4 Substructure-based model updating

The global flexibility estimated from the experimental testing is disassembled into the substructural flexibility matrices, which are thereafter used as references for updating the analytical models of the independent substructures. In the model updating procedure, superscript *E* represents the modal data from the experimental measurement, and *A* the data of the analytical model.

Taking Substructure 2 in Fig. 1 as an example, after the substructural flexibility matrix $\left(\overline{\mathbf{F}}_{aa}^{(2)}\right)^{E}$ is extracted from the global flexibility matrix $\left(\mathbf{F}_{g}\right)_{aa}^{E}$, the sub-model of Substructure 2 is updated independently as follows.

1) The rigid body modes $\mathbf{R}_{a}^{(2)}$ are constructed according to the nodal location of Substructure 2, and then orthogonal projector $\mathbf{P}_{a}^{(2)}$ is calculated (see Appendix).

2) The rigid body modes are removed from the generalized flexibility matrix $\left(\overline{\mathbf{F}}_{aa}^{(2)}\right)^{E}$ using orthogonal projector $\mathbf{P}_{a}^{(2)}$: $\left(\tilde{\mathbf{F}}_{aa}^{(2)}\right)^{E}=\left[\mathbf{P}_{a}^{(2)}\right]^{T}\left(\overline{\mathbf{F}}_{aa}^{(2)}\right)^{E}\mathbf{P}_{a}^{(2)}$.

3) The analytical model of Substructure 2 is updated by treating it as an independent structure.

The substructural flexibility matrix $\left(\mathbf{F}_{aa}^{(2)}\right)^{A}$ at the measured DOFs is calculated from the analytical model in each iteration and the orthogonal projector is multiplied as $\left(\tilde{\mathbf{F}}_{aa}^{(2)}\right)^{A} = \left[\mathbf{P}_{a}^{(2)}\right]^{T}\left(\mathbf{F}_{aa}^{(2)}\right)^{A}\mathbf{P}_{a}^{(2)}$. The elemental parameters in Substructure 2 are adjusted to minimize the difference of $\Delta\mathbf{F} = norm\left(\left(\tilde{\mathbf{F}}_{aa}^{(2)}\right)^{E} - \left(\tilde{\mathbf{F}}_{aa}^{(2)}\right)^{A}\right)$ through some optimization algorithms, for example the Trust Region Newton method [24].

5 Case study 1: A laboratory-tested portal frame structure

The effectiveness of the proposed substructuring method in model updating and damage identification is examined using a laboratory-tested steel frame structure. The dimensions of the frame are shown in Fig. 2; the cross section of the beam is 50.0 × 8.8 mm^2 and the columns are 50.0 × 4.4 mm^2. The mass density of the steel is 7.67 × 10^3 kg/m^3. The analytical model of the frame is composed of 44 nodes and 45 elements, labeled in Fig. 3. The global structure is separated into three substructures as shown in Fig. 4.

5.1 Convergence of the iterative process

The iteration convergence of the proposed substructuring method is verified in this section. The substructural flexibility matrix of a concerned substructure is extracted from the global modal data and compared with the real matrix obtained from the independent analytical model of the same substructure.

First the substructural flexibility matrix of the first substructure $\left(\tilde{\mathbf{F}}_{aa}^{(1)}\right)^{E}$ is extracted from the global modal data, while the analytical sub-models of the second and third substructures are assumed to be known in advance. For this purpose, the frequencies and mode shapes of the global structure are obtained from the global model (Fig. 3). The frequencies and mode shapes corresponding to the first substructure are used to construct the global flexibility matrix at the

measured points $\left(\mathbf{F}_g\right)_{aa}^{E}$, here the lateral directions of Nodes 1 to 18 in Fig. 3.

The substructural flexibility matrix $\left(\tilde{\mathbf{F}}_{aa}^{(1)}\right)^{E}$ is extracted using the global flexibility matrix $\left(\mathbf{F}_g\right)_{aa}^{E}$ by the proposed iterative scheme. In each iteration $\left(\tilde{\mathbf{F}}_{aa}^{(1)}\right)^{E}$ is compared with the actual flexibility matrix $\left(\tilde{\mathbf{F}}_{aa}^{(1)}\right)^{A}$, calculated from the analytical sub-model of the first substructure (Fig. 4). Their difference is evaluated as

$$Diff\left(\mathbf{F}\right)=\frac{norm\left(\left(\tilde{\mathbf{F}}_{aa}^{(1)}\right)^{E}-\left(\tilde{\mathbf{F}}_{aa}^{(1)}\right)^{A}\right)}{norm\left(\left(\tilde{\mathbf{F}}_{aa}^{(1)}\right)^{A}\right)} \tag{43}$$

where *norm*(·) gives the Frobenius norm of a matrix hereinafter. $Diff\left(\mathbf{F}\right)$ is less than a tolerance $Tol = 1\times10^{-6}$ after 32 iterations, as illustrated in Fig. 5(a). This indicates that the extracted substructural flexibility matrix $\left(\tilde{\mathbf{F}}_{aa}^{(1)}\right)^{E}$ can accurately reproduce the actual flexibility matrix $\left(\tilde{\mathbf{F}}_{aa}^{(1)}\right)^{A}$.

Next, the substructural flexibility matrix of the second substructure is extracted from the global modal data, while the sub-models of the first and third substructures are assumed to be available. The global structure is assumed to be measured at the second substructure to assemble $\left(\mathbf{F}_g\right)_{aa}^{E}$, including the measurements at lateral direction of Node 7 and Nodes 18 to 32.

$\left(\mathbf{F}_{aa}^{(2)}\right)^{E}$ is extracted from the global flexibility matrix $\left(\mathbf{F}_g\right)_{aa}^{E}$ in a similar iterative manner. Because the second substructure is free after partition, $\left(\mathbf{F}_{aa}^{(2)}\right)^{E}$ multiplies the orthogonal projector via $\left(\tilde{\mathbf{F}}_{aa}^{(2)}\right)^{E}=\mathbf{P}_{aa}^{(2)}\left(\mathbf{F}_{aa}^{(2)}\right)^{E}\mathbf{P}_{aa}^{(2)}$. For comparison, the real substructural flexibility matrix $\left(\mathbf{F}_{aa}^{(2)}\right)^{A}$ is calculated from the analytical sub-model of the second substructure and also multiplies the orthogonal projector as $\left(\tilde{\mathbf{F}}_{aa}^{(2)}\right)^{A}=\mathbf{P}_{aa}^{(2)}\left(\mathbf{F}_{aa}^{(2)}\right)^{A}\mathbf{P}_{aa}^{(2)}$. The difference between $\left(\tilde{\mathbf{F}}_{aa}^{(2)}\right)^{E}$

and $\left(\tilde{\mathbf{F}}_{aa}^{(2)}\right)^{A}$ is calculated by Eq. (43) in each iteration. Setting the tolerance to $Tol = 1\times10^{-6}$ again, the norm of the difference in each iteration is illustrated in Fig. 5(b).

Finally, the accuracy of the extracted substructural flexibility matrix of the third substructure is investigated. Details are not repeated here for brevity. The convergence process is illustrated in Fig. 5(c) with the identical tolerance of 1×10^{-6}.

Fig. 5 demonstrates that the substructural flexibility matrices extracted from the global modal data accurately reproduce the actual flexibility matrices of the independent substructures for all of the three substructures.

5.2 Refinement of the initial model

In this section, the substructural flexibility matrices of the three substructures are extracted from the experimental measurement data in the undamaged state, and are used as the reference for updating the three sub-models (Fig. 4).

Vibration testing on the global structure in the undamaged state is carried out in laboratory. The input and output time history data are recorded at the lateral direction of the measured nodes (Nodes 1 to 44 in Fig. 3) to derive the frequency response functions. Typical curves of the experimental measurements are illustrated in Fig. 6. Based on the measurement data, 14 pairs of natural frequencies and mass-normalized mode shapes are extracted by the rational fraction polynomial method [25]. Table 1 lists the measured frequencies. The global flexibility matrix is formulated, according to Eq. (29), from the 14 pairs of measured natural frequencies and mode shapes.

The proposed substructuring method is utilized to simultaneously extract the substructural flexibility matrices of substructures ($\left(\mathbf{F}_{aa}^{(1)}\right)^{E}$, $\left(\overline{\mathbf{F}}_{aa}^{(2)}\right)^{E}$, and $\left(\overline{\mathbf{F}}_{aa}^{(3)}\right)^{E}$). Because the second and

third substructures are free-free structures after partitioning, the extracted generalized flexibility matrices should multiply the orthogonal projector $\left(\tilde{\mathbf{F}}_{aa}^{(j)}\right)^{E}=\left[\mathbf{P}_{a}^{(j)}\right]^{T}\left(\bar{\mathbf{F}}_{aa}^{(j)}\right)^{E}\mathbf{P}_{a}^{(j)}$ (j=2, 3). The three substructural experimental flexibility matrices are then used as the bases in independently adjusting the updating parameters of the three sub-models in the undamaged state, according to the procedures described in Section 4. The elemental bending rigidities of all 45 elements are chosen as the updating parameters. Accordingly, there are 17 updating parameters in the first substructure, 15 in the second, and 13 in the third.

The elemental stiffness reduction factor (SRF) is employed to indicate the change ratio of the updated parameter to the initial value before updating [26].

$$\mathrm{SRF}=\frac{\Delta r}{r}=\frac{r^{U}-r^{O}}{r^{O}} \tag{44}$$

where superscript O represents the original parameters before updating and U represents the updated values after updating. Fig. 7 shows the SRF values of the three substructures after their respective sub-models are updated. To examine the correctness of the updated sub-models, the updated parameters are re-used in the global structure to calculate the frequencies and mode shapes of the global structure. The frequencies and modal assurance criterion (MAC) values of the mode shapes [26] before and after updating are compared with their measured counterparts in Table 1. The frequencies and mode shapes of the updated structure match the experimental results better than those before updating, indicating the updated substructural models are better at representing the actual structure. The three refined sub-models are used for damage identification in the subsequent section.

5.3 Damage detection based on the substructural approach

Two damage configurations are introduced in the frame. In the first damage case, the column of the first storey is cut at 180 mm away from the support (Fig. 2). The width of the cut is b = 10 mm, and depth d = 15 mm. Subsequently, the second storey is cut at 750 mm from the support with a width b = 10 mm and depth d = 15 mm.

In the first damage case, only the local measurement within the first storey, i.e., Nodes 1 to 18 in Fig. 3, is required because the cut is located in the first storey only. With modal testing, 14 pairs of frequencies and mass-normalized mode shapes are obtained, from which the global flexibility matrix in the damage state is formulated. Using the proposed substructuring method, only the substructural flexibility matrix of the first substructure is extracted.

The first substructure is updated independently to reproduce the extracted substructural flexibility matrix, without including the second and third substructures. Fig. 8 shows the SRF values of the 17 elements after updating. Element 2 shows a significant reduction in stiffness, in an agreement with the location of the cut in the experiment. The magnitude of SRF indicates the severity of element damage and represents the overall equivalent reduction in the element bending rigidity caused by the local cut. Other undamaged elements are identified with small SRFs ranging from 0 to –10%. This error may be due to measurement noise. Again, the updated parameters are used in the global structure, and the modal data of the global structure in this damage state are calculated and compared with the experimental modal data in Table 2. The updated model matches the experiment in the damaged state better than does the original model.

In the second damage configuration, two artificial cuts are respectively located in the first and second substructures. The frequencies and mode shapes measured in the first and second stories are used to form the global flexibility matrix, from which the substructural flexibility matrices of the first and second substructures are simultaneously extracted. The analytical sub-models of the first and second substructures are separately updated to recover the experimental counterparts. Fig. 9 shows that after updating, the SRF value of Element 2 in the first substructure is about –20% and the SRF value of Element 2 in the second substructure (Element 19 of the global structure) is –25%. The frequencies and MAC values in the updated model are compared with those before updating in Table 3; the updated model matches the experiment better than does the non-updated model.

In both damage configurations, the identified damage elements agree with the locations of the artificial cuts made in the experiment, indicating that the proposed substructuring method successfully localizes the artificial damage.

5.4 Damage detection based on the global approach

For comparison, the frame structure is updated using the traditional global method [16], in which the measured modal data are the same as those used in the substructure-based model updating method; that is, 14 pairs of frequencies and mode shapes are employed to formulate the global flexibility matrix in the undamaged state and two damaged states. The difference in the global flexibility matrices of the analytical model and experimental measurement is chosen as the objective function, and is used to simultaneously adjust the 45 elemental parameters. The initial model is first updated with the modal data measured in the undamaged state. The SRF values of the elemental parameters after updating are shown in Fig. 10. The refined model is subsequently used for damage identification.

The SRF values from the two damage configurations are illustrated in Figs. 11 and 12. Element 2 is observed to have a significantly negative SRF value in both damage configurations. The SRF value of Element 19 is about –30% in the second damage configuration. These observations are consistent with those obtained with the substructure-based model updating method (see Figs. 7–9). As a result, the proposed substructuring method is effective in model updating and damage identification.

In this small structure, the entire calculation is very rapid and the substructure-based model updating method has no advantage over the traditional global method in terms of computational efficiency. In the next section, a relatively larger structure, the Guangzhou New TV Tower, is chosen as an illustrative case in investigating the efficiency of the two model updating methods.

6 Case study 2: The Guangzhou New Television Tower

The Guangzhou New TV Tower is a supertall structure 600 m high. It consists of a main tower (454 m) and an antennary mast (146 m), as shown in Fig. 13(a). The main tower comprises a reinforced concrete inner tube and a steel outer tube of concrete-filled tube columns [27]. The analytical FE model of the structure [Fig. 13(b)] includes 8,738 three-dimensional elements, 3,671 nodes (each of which has six DOFs), and 21,690 DOFs [6].

The “experimental” frequencies and mode shapes are simulated on the global structure by intentionally reducing the bending rigidity of 48 column elements of the outer tube in the local area (denoted in Fig. 13) by 30%. The structure is measured at randomly selected 50 DOFs within the concerned local area, and the first 10 “experimental” modes are available. The mode shapes are normalized to the mass matrix. The “experimental” flexibility matrix is formed from the 10 frequencies and mode shapes.

The analytical model is updated employing both the traditional global-based model updating method and the proposed substructure-based model updating method for comparison. In this example, local area of the analytical model is updated using both the global-based model updating and substructure-based model updating. The bending rigidities of all the column elements of the outer tube in the concerned local area are chosen as the updating parameters. Accordingly, there are a total of 144 updating candidates.

First, the traditional global-based model updating method [16] is applied to update the analytical model, in which the difference between the analytical flexibility matrix and experimental flexibility matrix of the global structure is used as the objective function. The 144 updating parameters in the concerned local area of the analytical model are tuned to match the experimental measurement. The analytical flexibility matrix and its derivatives are calculated from the first 10 eigensolutions of the global FE model in each iteration. The system matrices of

the global FE model take the size 21,690 × 21,690. One iteration takes about 1.27 hours in an ordinary personal computer with a 2.8 GHz CPU and 2 GB memory. Setting the convergence criterion to be the norm of the objective function of 1×10^{-6}, the model updating process is completed after 15 iterations, and the entire process takes 17.88 hours. The convergence process in terms of the norm of the objective function is illustrated in Fig. 14.

Next, the proposed substructure-based model updating method is employed, in which the measurement data, updating parameters, optimization algorithm, and convergence criterion are the same as those used in the global-based approach. The global structure is divided into 10 substructures along the vertical direction as in Fig. 13(c). The global "experimental" flexibility is disassembled into the substructural flexibility matrix for the concerned substructure, taking about 531.4 seconds. Subsequently, the FE model of the concerned substructure (Fig. 13(d)] is updated independently to reproduce the substructural "experimental" flexibility matrix. The FE model of the concerned substructure is composed of 945 elements, 456 nodes, and 2,736 DOFs. In each iteration, the substructural flexibility and its derivative matrix are calculated from the first 10 eigensolutions of the substructural model, whose system matrices take the size of 2,736×2,736. Given that the substructural model has a size much smaller than that of the global structure, the substructure-based model updating performs much faster than the global method. In particular, one iteration takes only about 0.11 hours and the entire process takes 1.69 hours, less than 10% of that consumed in the traditional global method. The substructure-based model updating process is completed within 14 iterations in satisfying the convergence criterion of 1×10^{-6}; the convergence process is illustrated in Fig. 14. For comparison, the norm values from the two methods in Fig. 14 are normalized with the maximum value of 1. With regard to the computational time in the model updating of a large-scale structure, the time consumed in extracting the substructural experimental flexibility matrix from the global experimental flexibility is negligible.

The frequencies and mode shapes of the updated structure are compared with the values before updating (Table 4). The experimental eigenmodes are simulated numerically without considering

the measurement noise. Consequently the updated FE models precisely recover the "experimental" counterparts exactly.

In the above analysis, the local area is updated when the location of local damage is known in priori. 144 parameters are tuned for both the substructure- and global-based model updating. The global structure has 1104 column elements in total. If the damage is not known in priori, all 1104 column elements have to be tuned through the model updating process. In this regards, the flexibility matrices of each substructure will be extracted at the same time. Then model updating is independently conducted on 10 substructures one by one. Each substructure has about one hundred updating parameters. The computation time in extraction and updating all 10 substructures is about 10 times of that for one substructure, that is, 10 × 1.69 hours. On the other hand, the global method needs to simultaneously update 1104 parameters at one time. The large number of updating parameters will heavily hinder the convergence of the model updating. The computation time shall be about 10 times updating one local area, that is, 10 × 17.88 hours. Again the proposed substructuring method is very computational efficient, as compared with the conventional global-based model updating.

7 Conclusions

This paper proposes a new inverse substructure-based model updating method. The global flexibility matrix from the experiments is disassembled into the substructural flexibility matrices, which are then employed as references for updating the sub-models of the independent substructures. Because only the concerned substructure is adjusted in model updating, the proposed substructuring method reduces the size of the analytical model involved and decreases the uncertain parameters, thereby improving the computational efficiency of the optimization process. In addition, the proposed substructuring method requires the measurement of only the local area of the concerned substructures.

The accuracy and effectiveness of the proposed method in model updating and damage detection are verified through application to a laboratory-tested frame structure. The proposed method can successfully detect the damages using the measurement of the local area, and the identification results are similar to those obtained through the conventional global-based model updating method.

The efficiency of the proposed updating process is numerically demonstrated through a large-scale structure. The substructure-based model updating procedure is much faster than the traditional global-based procedure. The proposed substructure-based model updating method exhibits promising prospects in releasing the computational load of large-scale structures.

Acknowledgments

This work is jointly supported by a grant from the Research Grants Council of the Hong Kong Special Administrative Region, China (Project No. PolyU 5321/08E) and a grant from the National Natural Science Foundation of China (No.51108205 and No. 50925828).

References

[1] J.M.W. Brownjohn, P.Q. Xia, H. Hao, Y. Xia, Civil structure condition assessment by FE model updating: methodology and case studies, *Finite Elements in Analysis and Design*, 37 (2001) 761-775.

[2] Y. Xia, H. Hao, A.J. Deeks, X.Q. Zhu, Condition assessment of shear connectors in slab-girder bridges via vibration measurements, *Journal of Bridge Engineering*, 13 (2008) 43-54.

[3] Y.F. Duan, Y.L. Xu, Q.G. Fei, K.Y. Wong, K.W.Y. Chan, Y.Q. Ni, Full 3D finite element model for criticality analysis of Tsing Ma Bridge, *International Conference on Bridge Engineering*, Hong Kong, 2006.

[4] S. Weng, Y. Xia, Y.L. Xu, X.Q. Zhou, H.P. Zhu, Improved substructuring method for eigensolutions of large-scale structures, *Journal of Sound and Vibration*, 323 (2009)

718-736.

[5] Y. Xia, S. Weng, Y.L. Xu, H.P. Zhu, Calculation of eigenvalue and eigenvector derivatives with the improved Kron's substructuring method, *Structural Engineering and Mechanics*, 36 (2010) 37-55.

[6] S. Weng, Y. Xia, Y.L. Xu, H.P. Zhu, An iterative substructuring approach to the calculation of eigensolution and eigensensitivity, *Journal of Sound and Vibration*, 330 (2011) 3368-3380.

[7] S. Weng, Y. Xia, Y.L. Xu, H.P. Zhu, Substructure based approach to finite element model updating, *Computers and Structures*, 89 (2011) 772-782.

[8] R.R. Craig, S.E.M. Sem, A brief tutorial on substructure analysis and testing, *The 18th IMAC Conference on Computational Challenges in Structural Dynamics*, San Antonio, TX, 2000, pp. 899-908.

[9] M. Lou, A. Ghobarah, T.S. Aziz, Application of Wilson-Ritz vectors in dynamic substructuring, *International Journal of Solids and Structures*, 30 (1993) 3159-3170.

[10] D. Choi, H. Kim, M. Cho, Iterative method for dynamic condensation combined with substructuring scheme, *Journal of Sound and Vibration*, 317 (2008) 199-218.

[11] K.F. Alvin, K.C. Park, Extraction of substructural flexibility from global frequencies and mode shapes, *AIAA Journal*, 37 (1999) 1444-1451.

[12] S.W. Doebling, L.D. Peterson, Experimental determination of local structural stiffness by disassembly of measured flexibility matrices, *Journal of Vibration and Acoustics*, 120 (1998) 949-957.

[13] C.G. Koh, B. Hong, C.Y. Liaw, Substructural and progressive structural identification methods, *Engineering Structures*, 25 (2003) 1551-1563.

[14] S.S. Law, K. Zhang, Z.D. Duan, Structural damage detection from coupling forces between substructures under support excitation, *Engineering Structures*, 32 (2010) 2221-2228.

[15] Z. Duan, G. Yan, J. Ou, B.F. Spencer, Damage detection in ambient vibration using proportional flexibility matrix with incomplete measured DOFs, *Structural Control and Health Monitoring*, 14 (2005) 186-196.

[16] B. Jaishi, W.X. Ren, Damage detection by finite element model updating using modal flexibility residual, *Journal of Sound and Vibration*, 290 (2006) 369-387.

[17] T.S. Shores, *Applied Linear Algebra and Matrix Analysis*. New York : Springer Science + Business Media, LLC, 2007.

[18] F. Liu, D.W. Zhang, L. Zhang, Dynamic flexibility method for extracting constrained structural modes from free test data, *AIAA Journal*, 39 (2001) 279-284.

[19] N.S. Sehmi, *Large Order Structural Eigenanalysis Techniques Algorithms for Finite*

Element Systems, Ellis Horwood Limited: Chichester, England, 1989.

[20] C.R. Rao, S.K. Mitra, *Generalized Inverse of Matrices and its Applications*, John Wiley & Sons, INC., 1971.

[21] A.N. Ng'andu, C.H.J. Fox, E.G. Williams, On the estimation of rotational degrees of freedom using spline functions, *Proceedings of the 13th International Modal Analysis Conference (IMAC 13)*, Nashville, TN, 1995.

[22] C.G. Koh, K. Shankar, Substructural identification method without interface measurement, *Journal of Engineering Mechanics*, 129 (2003) 769-776.

[23] Y. Xia, R.M. Lin, A new iterative order reduction (IOR) method for eigensolutions of large structures, *International Journal for Numerical Method in Engineering*, 59 (2004) 153-172.

[24] P.G. Bakir, E. Reynders, G. De Roeck, Sensitivity-based finite element model updating using constrained optimization with a trust region algorithm, *Journal of Sound and Vibration*, 305 (2007) 211-225.

[25] D.L. Formenti, M.H. Richardson, Parameter estimation from frequency response measurements using rational fraction polynomials, *The 20th International Modal Analysis Conference*, Los Angeles, CA, 2002, pp. 1-10.

[26] M.I. Friswell, J.E. Mottershead, *Finite Element Model Updating in Structural Dynamics*, Kluwer Academic Publishers, 1995.

[27] Y.Q. Ni, Y. Xia, W.Y. Liao, J.M. Ko, Technology innovation in developing the structural health monitoring system for Guangzhou New TV Tower, *Structural Control and Health Monitoring*, 16 (2009) 73-98.

Appendix: The orthogonal projector

In substructure-based FE model updating, the substructural flexibility matrix extracted from the measured global flexibility and that calculated from the analytical substructural model are compared. For a free substructure, the generalized flexibility matrix extracted using the proposed substructuring method is contributed by both the rigid body modes and deformational modes as Eq. (3).

$$\overline{\mathbf{F}} = \mathbf{\Phi}_d \mathbf{\Lambda}_d^{-1} \mathbf{\Phi}_d^T + \mathbf{R}\mathbf{A}\mathbf{R}^T \tag{a1}$$

where $\overline{\mathbf{F}}$ is the generalized flexibility, and conventional flexibility $\mathbf{F} = \mathbf{\Phi}_d \mathbf{\Lambda}_d^{-1} \mathbf{\Phi}_d^T$ includes only the deformational modes. Removing the rigid body components from the generalized

substructural flexibility is necessary to make the substructural flexibility matrix calculated from the analytical substructural model and that extracted from the global flexibility comparable. In the following section, an orthogonal projector is constructed to remove the rigid body components.

A general free structure, with stiffness matrix **K** and mass matrix **M**, can be described by the eigenequation

$$\left(\mathbf{K}-\lambda\mathbf{M}\right)\mathbf{\Phi}=\mathbf{0} \tag{a2}$$

This eigenequation has two kinds of eigenpairs: N_r zero eigenvalues associated with rigid body modes **R**, and N_d nonzero eigenvalues associated with deformational modes $\mathbf{\Phi}_d$. They satisfy the orthogonality condition

$$\mathbf{R}^T\mathbf{M}\mathbf{R}=\mathbf{I},\ \ \mathbf{\Phi}_d^T\mathbf{M}\mathbf{\Phi}_d=\mathbf{I},\ \ \mathbf{R}^T\mathbf{M}\mathbf{\Phi}_d=\mathbf{0} \tag{a3}$$

Concerning the orthogonal property in Eq. (a3), an orthogonal projector **P** can be constructed as

$$\mathbf{P}=\mathbf{I}-\mathbf{M}\mathbf{R}\mathbf{R}^T=\mathbf{M}\mathbf{\Phi}_d\mathbf{\Phi}_d^T \tag{a4}$$

which satisfies

$$\mathbf{P}^2=\mathbf{P}\left(\mathbf{I}-\mathbf{M}\mathbf{R}\mathbf{R}^T\right)=\left(\mathbf{I}-\mathbf{M}\mathbf{R}\mathbf{R}^T\right)\mathbf{P}=\mathbf{P},\ \ \left(\mathbf{M}\mathbf{R}\right)^T\mathbf{P}=\mathbf{0},\ \ \mathbf{P}\mathbf{M}\mathbf{R}=\mathbf{0} \tag{a5}$$

Projector **P** can filter out the rigid body components, and leaves only the deformational modes in the generalized flexibility matrix by

$$\begin{aligned}\tilde{\mathbf{F}}&=\mathbf{P}^T\bar{\mathbf{F}}\mathbf{P}=\left(\mathbf{I}-\mathbf{M}\mathbf{R}\mathbf{R}^T\right)^T\left(\mathbf{\Phi}_d\mathbf{\Lambda}_d^{-1}\mathbf{\Phi}_d^T+\mathbf{R}\mathbf{A}\mathbf{R}^T\right)\left(\mathbf{I}-\mathbf{M}\mathbf{R}\mathbf{R}^T\right)\\&=\left(\mathbf{\Phi}_d\mathbf{\Lambda}_d^{-1}\mathbf{\Phi}_d^T\right)\left(\mathbf{I}-\mathbf{M}\mathbf{R}\mathbf{R}^T\right)=\mathbf{\Phi}_d\mathbf{\Lambda}_d^{-1}\mathbf{\Phi}_d^T=\mathbf{F}\end{aligned} \tag{a6}$$

This equation implies that projector **P** can remove all the rigid body components from a generalized flexibility matrix regardless of any magnitude of the participation factors. Orthogonal projector **P** can be formulated in a variety of ways, provided that it is orthogonal to the rigid body modes; that is, the product of $\mathbf{R}\mathbf{R}^T$ and **P** is a zero matrix [17, 20].

Rigid body modes **R** are determined by the nodal location of a structure. For a two-dimensional

free structure having N nodes, the three independent rigid body modes are the x translation, y translation, and z rotation, that is,

$$\mathbf{R}^T = \begin{bmatrix} 1 & 0 & 0 & 1 & \cdots & 0 & 0 \\ 0 & 1 & 0 & 0 & \cdots & 1 & 0 \\ -y_1 & x_1 & 1 & -y_2 & \cdots & x_N & 1 \end{bmatrix} \tag{a7}$$

Consequently, orthogonal projector **P** is determined by the geometric dimension of a structure as well. Orthogonal projector **P** remains unchanged throughout the entire model updating process.

When the global structure is measured at partial DOFs, the extracted substructural flexibility is obtained at the DOFs corresponding to the measured ones only. Accordingly, the generalized flexibility extracted at the measured DOFs is written as

$$\overline{\mathbf{F}}_{aa} = \mathbf{\Phi}_{ad}\mathbf{\Lambda}^{-1}\mathbf{\Phi}_{ad}^T + \mathbf{R}_a\mathbf{A}\mathbf{R}_a^T \tag{a8}$$

Next, a condensed orthogonal projector is formulated to remove the rigid body components from the partial generalized flexibility matrix. For this purpose, a matrix that is mathematically orthogonal to reduced rigid body modes $\mathbf{R}_a$ is required.

The condensed model proposed by Xia et al. [23] is employed.

$$\mathbf{K}_{Red}\hat{\mathbf{\Phi}}_a = \hat{\lambda}\mathbf{M}_{Red}\hat{\mathbf{\Phi}}_a \tag{a9}$$

The eigenmodes ($\hat{\mathbf{\Phi}}_a$) of the reduced model consist of two parts: the rigid body modes at the measured DOFs $\mathbf{R}_a$ and the deformational modes at the measured DOFs $\hat{\mathbf{\Phi}}_{ad}$. In Eq. (a9), $\mathbf{K}_{Red} = \mathbf{K}_{aa} - \mathbf{K}_{ab}\mathbf{K}_{bb}^{-1}\mathbf{K}_{ba}$ is the condensed stiffness matrix, while condensed mass matrix $\mathbf{M}_{Red}$ is obtained through an iterative scheme [23].

In this reduced model, the rigid body modes and deformational modes satisfy the orthogonality condition

$$\mathbf{R}_a^T\mathbf{M}_{Red}\mathbf{R}_a = \mathbf{I}, \quad \hat{\mathbf{\Phi}}_{ad}^T\mathbf{M}_{Red}\hat{\mathbf{\Phi}}_{ad} = \mathbf{I}, \quad \mathbf{R}_a^T\mathbf{M}_{Red}\hat{\mathbf{\Phi}}_{ad} = \mathbf{0} \tag{a10}$$

Because of these orthogonal properties, condensed projector $\mathbf{P}_a$ is constructed as

$$\mathbf{P}_a = \mathbf{I} - \mathbf{M}_{Red}\mathbf{R}_a\mathbf{R}_a^T = \mathbf{M}_{Red}\hat{\mathbf{\Phi}}_{ad}\hat{\mathbf{\Phi}}_{ad}^T \tag{a11}$$

$$\mathbf{R}_a^T\mathbf{P}_a = \mathbf{P}_a^T\mathbf{R}_a = \mathbf{0} \tag{a12}$$

In this case, projector $\mathbf{P}_a$ is used to remove the rigid body modes of the generalized flexibility by

$$\mathbf{P}_a^T\overline{\mathbf{F}}_{aa}\mathbf{P}_a = \left(\mathbf{I} - \mathbf{M}_{Red}\mathbf{R}_a\mathbf{R}_a^T\right)^T\left(\mathbf{F}_{aa} + \mathbf{R}_a\mathbf{A}\mathbf{R}_a^T\right)\left(\mathbf{I} - \mathbf{M}_{Red}\mathbf{R}_a\mathbf{R}_a^T\right)$$

$$= \left(\mathbf{M}_{Red}\hat{\mathbf{\Phi}}_{ad}\hat{\mathbf{\Phi}}_{ad}^T\right)^T\mathbf{F}_{aa}\left(\mathbf{M}_{Red}\hat{\mathbf{\Phi}}_{ad}\hat{\mathbf{\Phi}}_{ad}^T\right) = \tilde{\mathbf{F}}_{aa} = \mathbf{P}_a^T\mathbf{F}_{aa}\mathbf{P}_a \tag{a13}$$

$\tilde{\mathbf{F}}_{aa}$ no longer contains the rigid body components. The resulting matrix $\tilde{\mathbf{F}}_{aa}$ can be compared with the analytical counterparts for model updating.

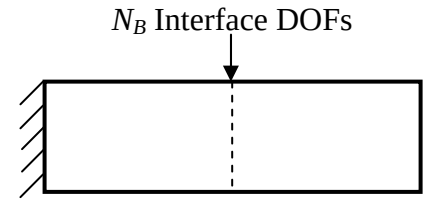

(a) Global structure

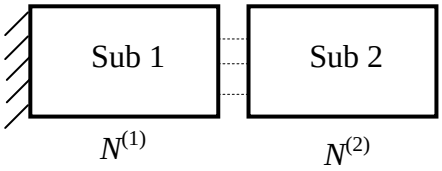

(b) Divided substructures

Fig. 1. Configuration of a structure with two substructures.

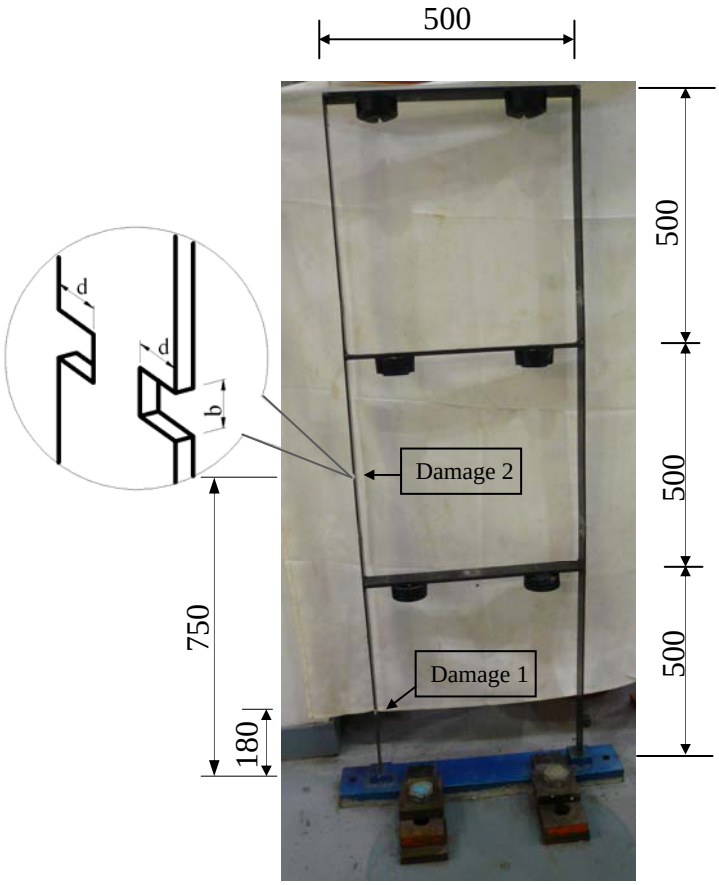

Fig. 2. Overview of the frame structure and the experimental damage configuration (unit: mm).

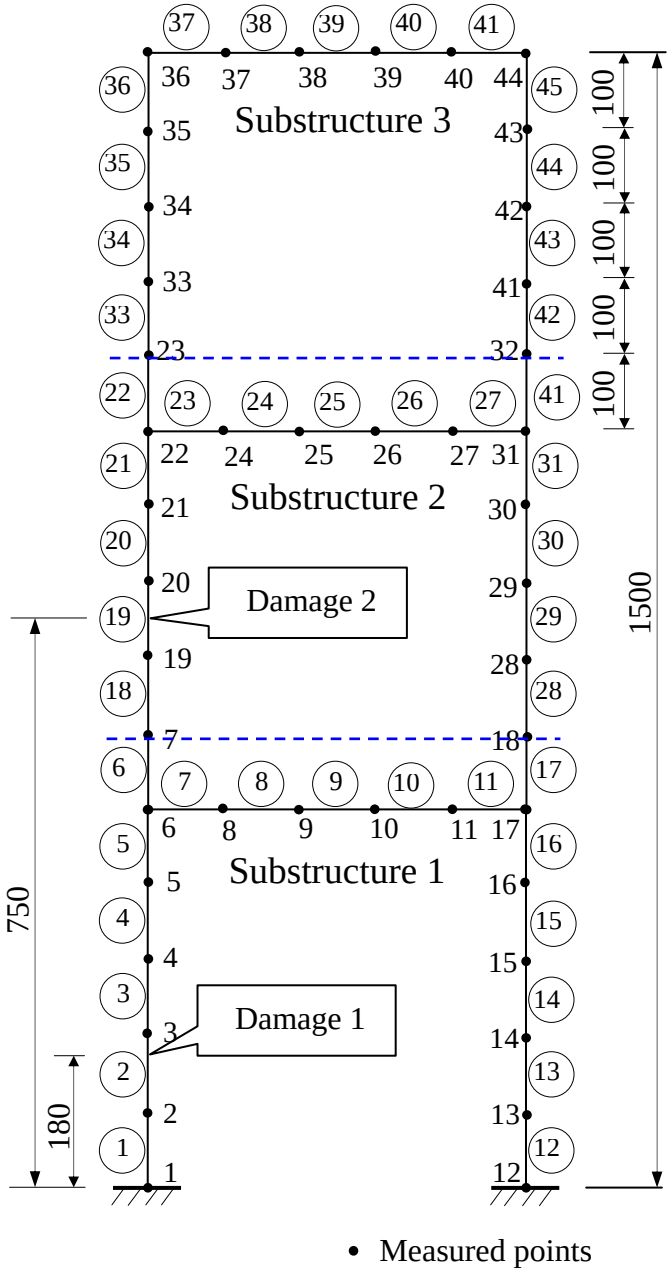

Fig. 3. Analytical model of the frame structure (unit: mm).

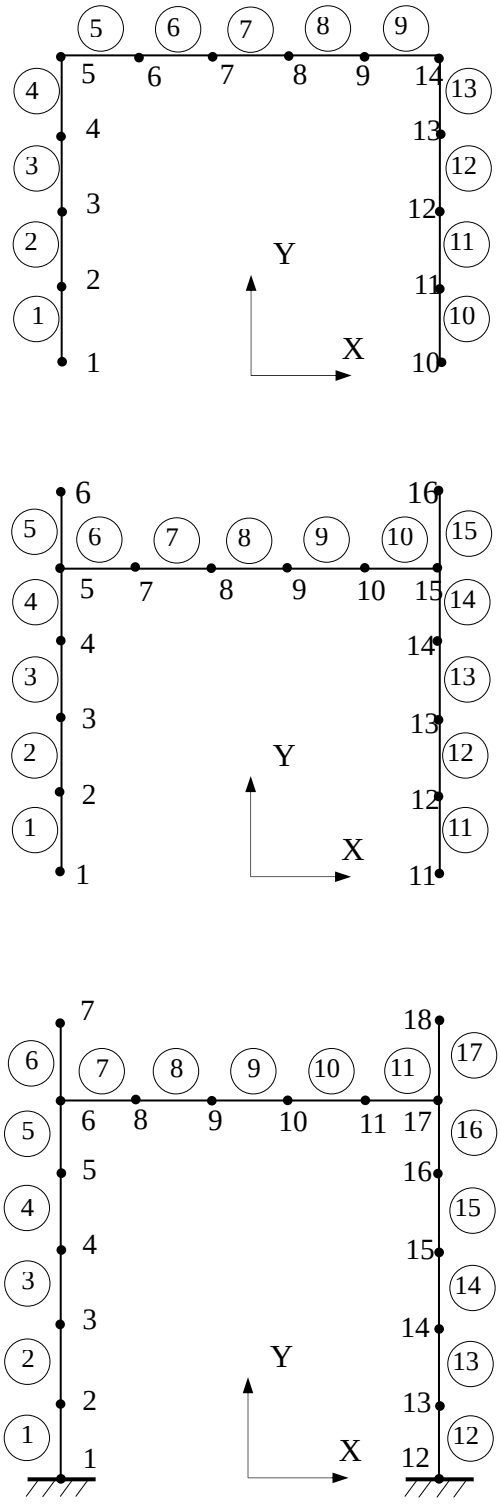

Fig. 4. Independent models of the three substructures.

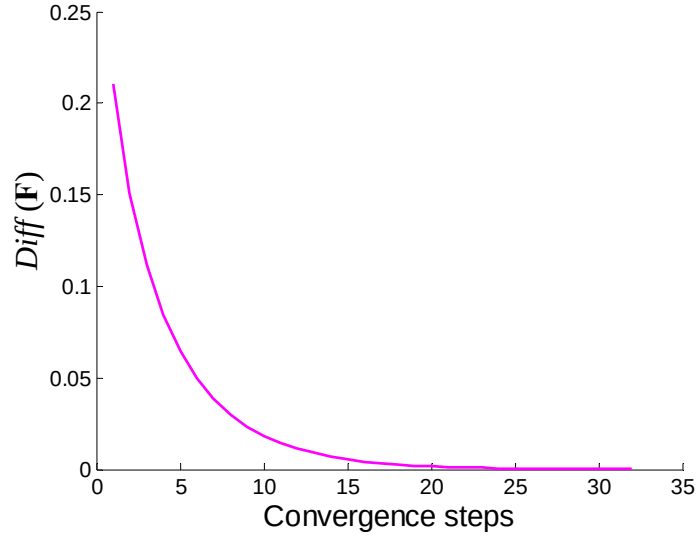

(a) Substructure 1

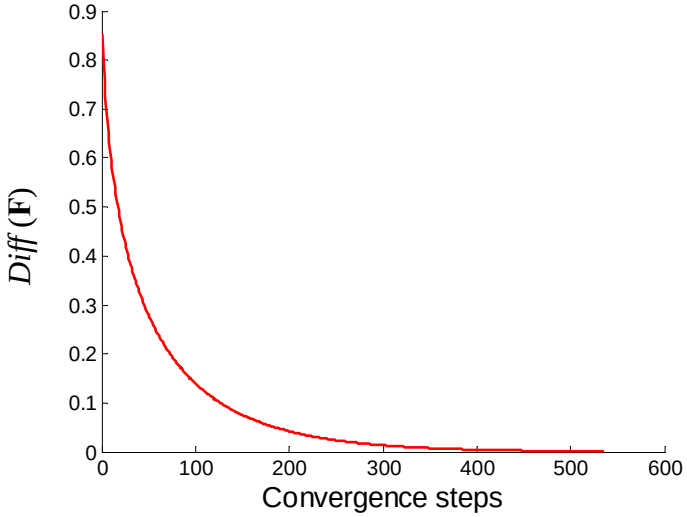

(b) Substructure 2

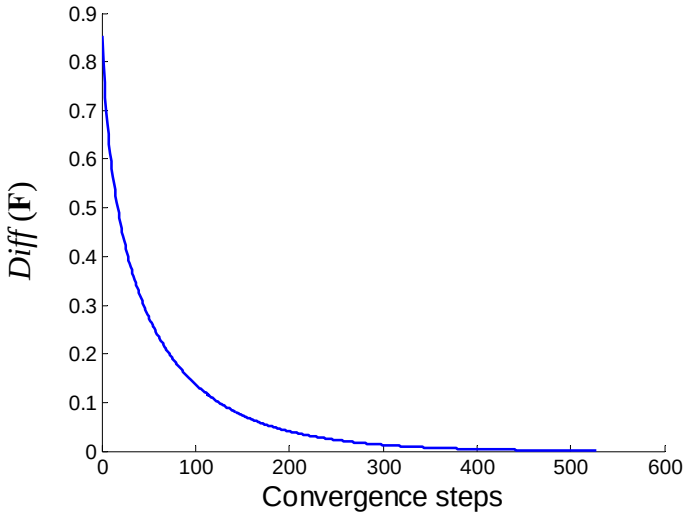

(c) Substructure 3

Fig. 5. Convergence of the Substructural Flexibility Matrix

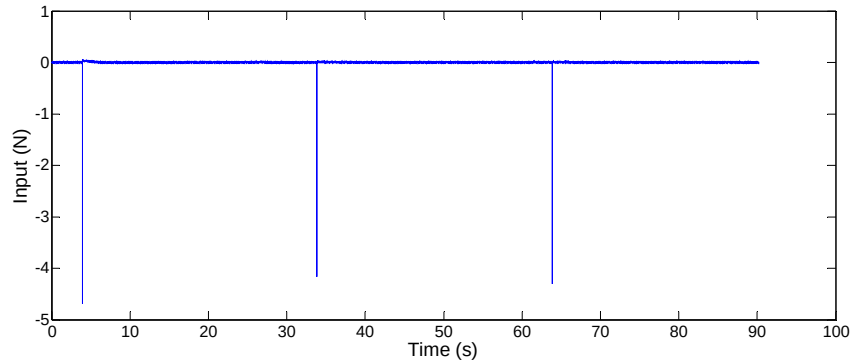

(a) Input Force Time History

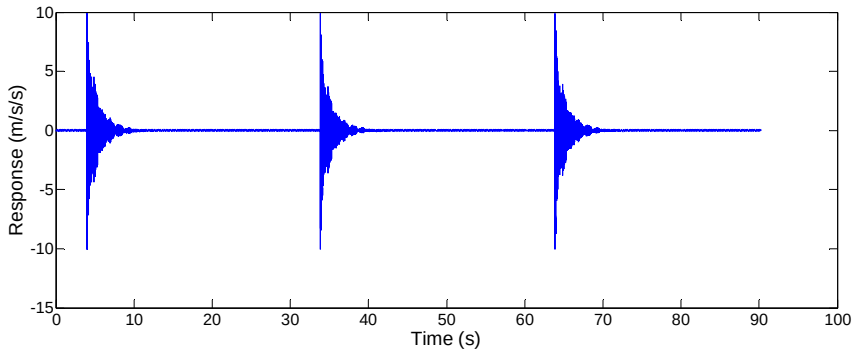

(b) Recorded Acceleration Time History at One Point

Fig. 6. Typical curves of the modal experiment

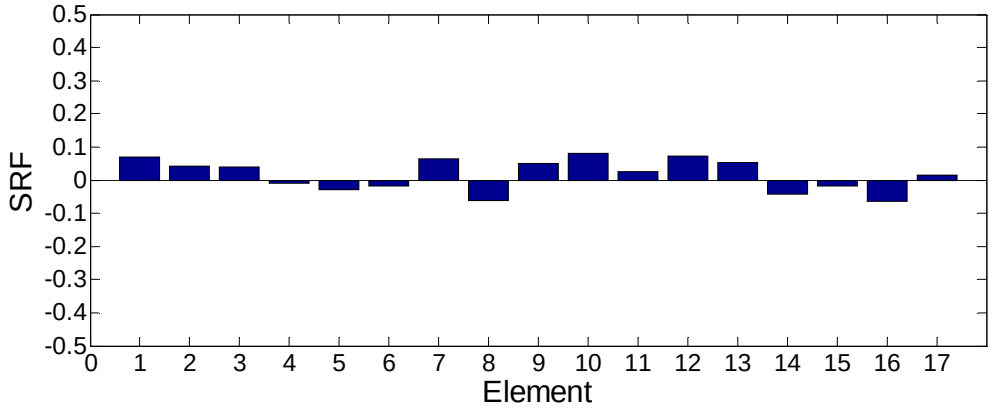

(a) First substructure

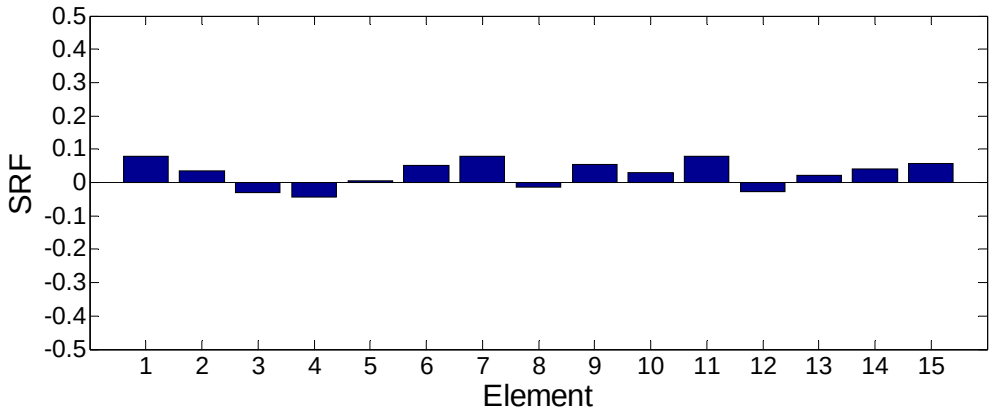

(b) Second substructure

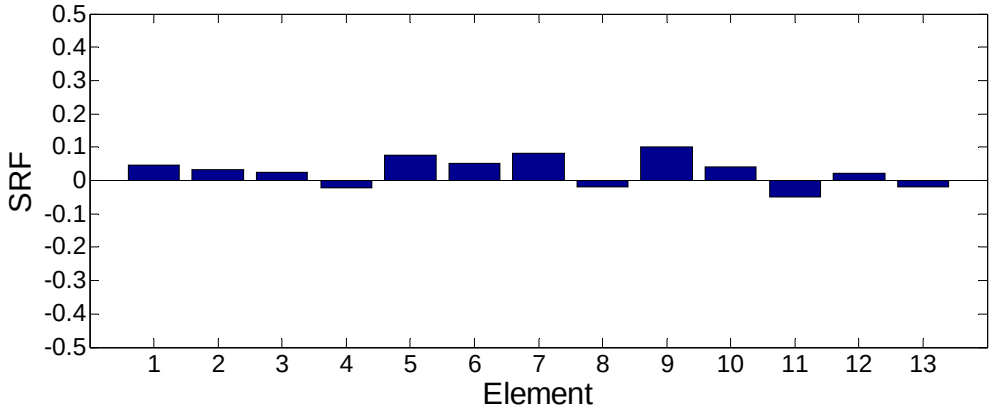

(c) Third substructure

Fig. 7. SRF values of the three substructures in the undamaged state.

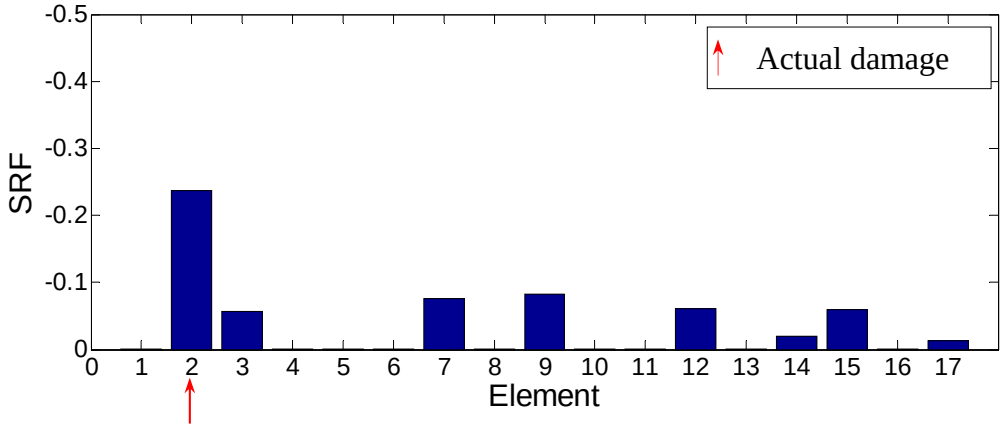

Fig. 8. SRF values of the first damage configuration (first substructure).

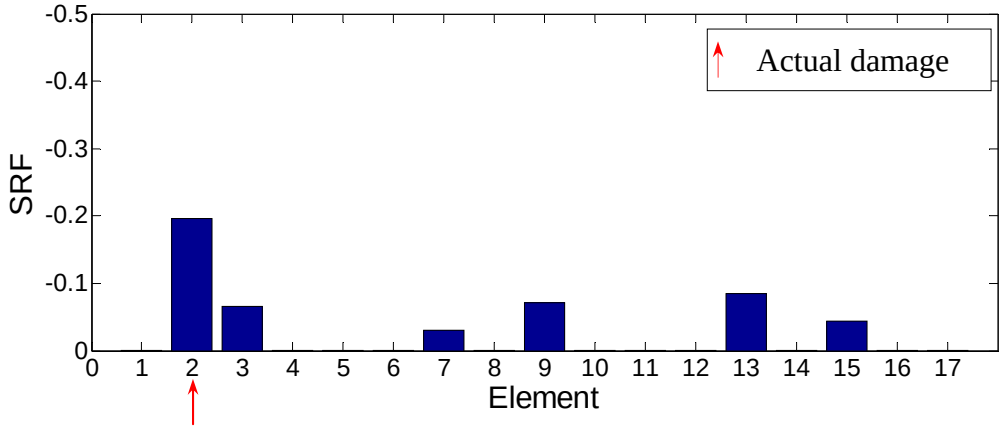

(a) First substructure

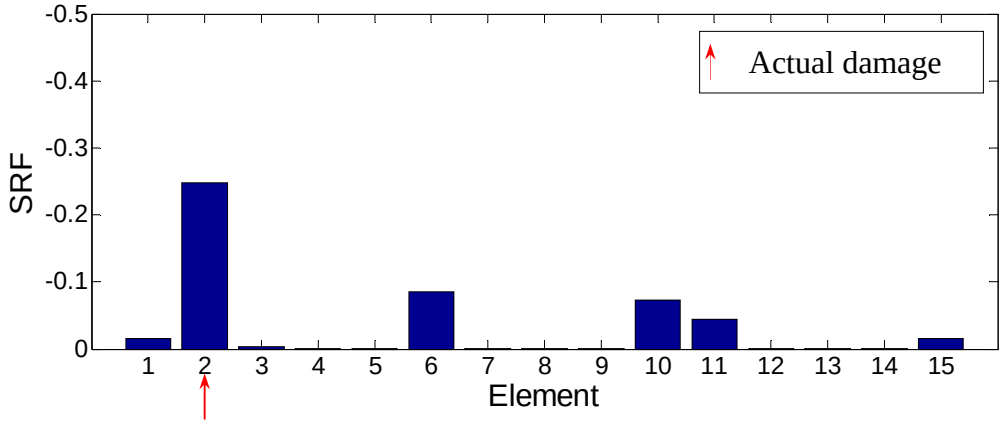

(b) Second substructure

Fig. 9. SRF values of the second damage configuration.

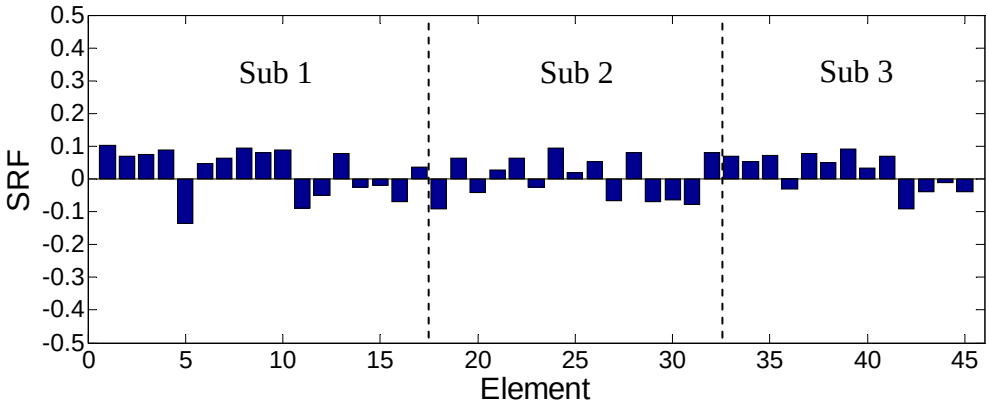

Fig. 10. SRF values of the frame structure in the undamaged state (global method).

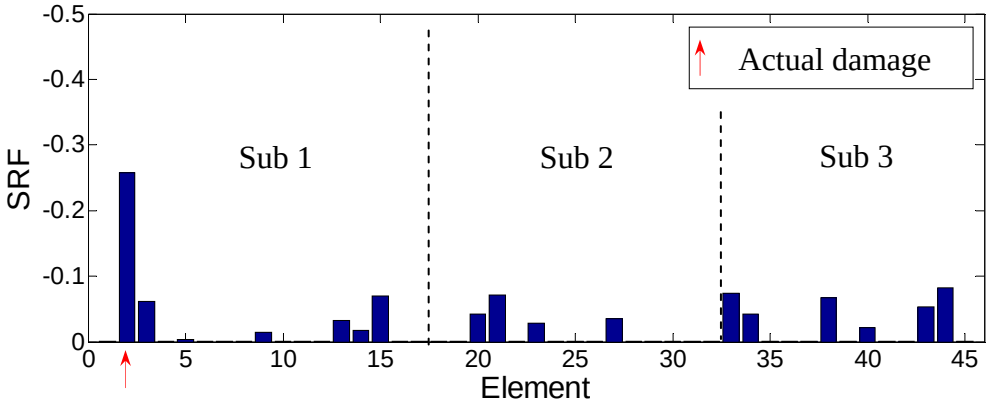

Fig. 11. SRF values of the first damage configuration (global method).

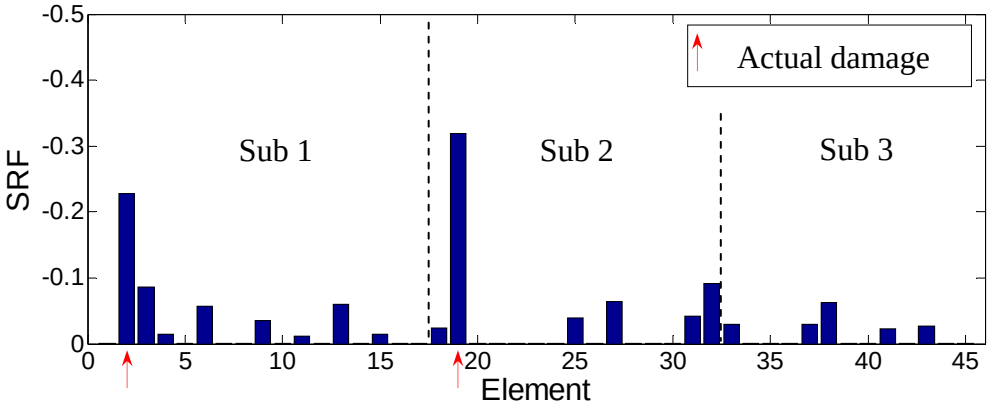

Fig. 12. SRF values of the second damage configuration (global method).

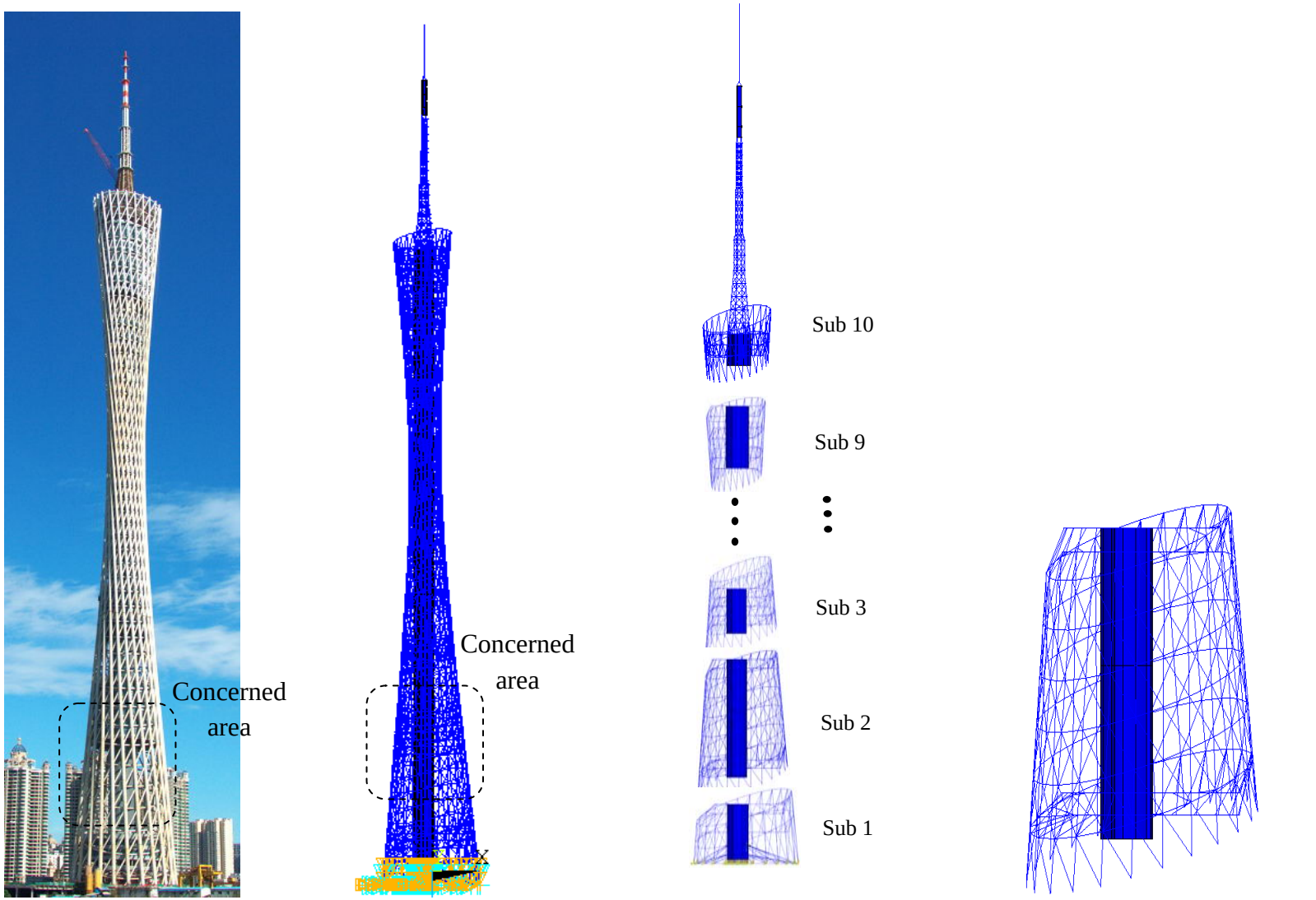

(a) Landscape view (b) Global model (c) Divided substructures (d) Concerned substructure

Fig. 13. Guangzhou New Television Tower and the FE model.

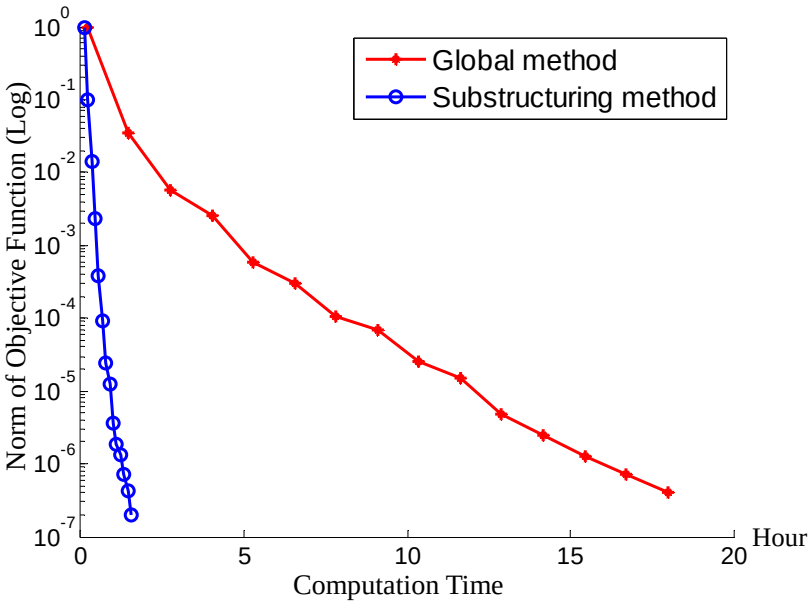

Fig. 14. Model updating process using the global and substructuring methods.

Table 1

Frequencies and mode shapes before and after updating (Undamaged state).

Mode	Analytical mode	Measured frequency (Hz)	Before updating			After updating		
			Freq. (Hz)	Diff. (%)	MAC	Freq. (Hz)	Diff. (%)	MAC
1	1	3.12	3.16	1.27%	0.993	3.13	0.32%	0.997
2	2	9.11	9.23	1.27%	0.976	9.15	0.44%	0.996
3	3	14.34	14.04	-2.13%	0.989	14.40	0.39%	0.993
4	4	52.46	50.42	-3.88%	0.981	51.90	-1.07%	0.997
5	5	58.18	56.51	-2.87%	0.980	57.74	-0.75%	0.989
6	6	66.80	64.34	-3.68%	0.871	66.84	0.06%	0.951
7	7	71.65	70.80	-1.18%	0.928	72.00	0.49%	0.970
8	8	82.14	82.51	0.45%	0.877	81.78	-0.43%	0.933
9	9	82.87	80.98	-2.29%	0.885	82.41	-0.55%	0.975
10	16	200.13	211.12	5.49%	0.919	205.54	2.70%	0.957
11	17	222.36	215.91	-2.90%	0.920	224.62	1.02%	0.965
12	18	226.55	220.37	-2.73%	0.913	226.13	-0.18%	0.959
13	19	236.58	230.60	-2.53%	0.905	235.17	-0.60%	0.959
14	22	383.33	395.44	3.16%	0.903	389.95	1.73%	0.951
Average of absolute values				2.56%	0.932		0.77%	0.971

Table 2

Frequencies and mode shapes before and after updating (damage case 1)

Mode	Analytical mode	Measured frequency (Hz)	Before updating			After updating		
			Freq. (Hz)	Diff. (%)	MAC	Freq. (Hz)	Diff. (%)	MAC
1	1	3.11	3.13	0.62%	0.992	3.11	-0.10%	0.992
2	2	9.09	9.15	0.64%	0.996	9.18	0.94%	0.997
3	3	14.34	14.40	0.42%	0.997	14.14	-1.39%	0.997
4	4	52.24	51.90	-0.65%	0.986	52.26	0.04%	0.985
5	5	57.72	57.74	0.03%	0.991	57.85	0.22%	0.992
6	6	66.73	66.84	0.18%	0.916	66.76	0.05%	0.949
7	7	71.28	72.00	1.01%	0.970	71.13	-0.21%	0.980
8	8	81.60	81.78	0.22%	0.860	81.67	0.09%	0.919
9	9	82.19	82.41	0.28%	0.859	82.29	0.13%	0.917
10	16	199.70	205.54	2.93%	0.932	200.90	0.60%	0.944
11	17	220.93	224.62	1.67%	0.847	221.47	0.24%	0.915
12	18	224.97	226.13	0.52%	0.840	225.07	0.04%	0.927
13	19	234.78	235.17	0.16%	0.947	233.58	-0.51%	0.973
14	22	382.50	389.95	1.95%	0.926	387.54	1.32%	0.949
Average of absolute values				0.81%	0.933		0.42%	0.960

Table 3
Frequencies and mode shapes before and after updating (damage case 2)

Mode	Analytical mode	Measured frequency (Hz)	Before updating			After updating		
			Freq. (Hz)	Diff. (%)	MAC	Freq. (Hz)	Diff. (%)	MAC
1	1	3.11	3.13	0.77%	0.992	3.10	-0.36%	0.996
2	2	9.09	9.15	0.67%	0.996	9.11	0.21%	0.998
3	3	14.33	14.40	0.46%	0.997	14.29	-0.33%	0.997
4	4	51.88	51.90	0.04%	0.988	51.47	-0.80%	0.985
5	5	57.41	57.54	0.23%	0.989	57.56	0.27%	0.986
6	6	66.48	66.84	0.54%	0.924	65.84	-0.97%	0.938
7	7	70.73	72.00	1.80%	0.961	70.88	0.21%	0.978
8	8	80.99	81.78	0.98%	0.838	81.17	0.23%	0.933
9	9	81.98	82.41	0.54%	0.889	82.20	0.27%	0.916
10	16	199.11	205.54	3.23%	0.912	200.51	0.70%	0.933
11	17	220.03	224.62	2.08%	0.839	220.95	0.42%	0.922
12	18	224.14	226.13	0.89%	0.819	223.33	-0.36%	0.926
13	19	233.50	235.17	0.71%	0.934	230.65	-1.22%	0.952
14	22	376.49	389.95	3.58%	0.859	382.54	1.61%	0.941
Average of absolute values				1.18%	0.924		0.57%	0.957

Table 4
Frequencies and mode shapes of the Guangzhou New TV Tower structure before and after updating

Mode	Measured Freq. (Hz)	Before updating			After updating (global method)			After updating (substructuring method)		
		Freq. (Hz)	Diff. (%)	MAC	Freq. (Hz)	Diff. (%)	MAC	Freq. (Hz)	Diff. (%)	MAC
1	0.111	0.112	1.05%	0.9975	0.111	0.00%	1.0000	0.111	0.00%	1.0000
2	0.161	0.163	1.25%	0.9969	0.161	0.00%	1.0000	0.161	0.00%	1.0000
3	0.344	0.344	0.05%	0.9997	0.344	0.00%	1.0000	0.344	0.00%	1.0000
4	0.372	0.376	0.95%	0.9993	0.372	0.00%	1.0000	0.372	0.00%	1.0000
5	0.406	0.406	0.12%	0.9989	0.406	0.00%	1.0000	0.406	0.00%	1.0000
6	0.429	0.431	0.33%	0.9997	0.429	0.00%	1.0000	0.429	0.00%	0.9999
7	0.493	0.496	0.66%	0.9996	0.493	0.00%	1.0000	0.493	0.00%	1.0000
8	0.696	0.697	0.18%	0.9991	0.696	0.00%	1.0000	0.696	0.00%	1.0000
9	0.818	0.818	0.03%	0.9992	0.818	0.00%	1.0000	0.818	0.00%	0.9999
10	0.868	0.869	0.06%	0.9994	0.868	0.00%	0.9999	0.868	0.00%	0.9999
Average			0.47%	0.9989		0.00%	1.0000		0.00%	1.0000